AD-A132 354 WEAR DURING RUBBING OF A SINTERED METAL POWDER BODY(U) 1/2
AIR FORCE INST OF TECH WRIGHT-PATTERSON AFB OH
J R ROGACKI 1983 AFIT/CI/NR-83-34T

UNCLASSIFIED F/G 11/6 NL

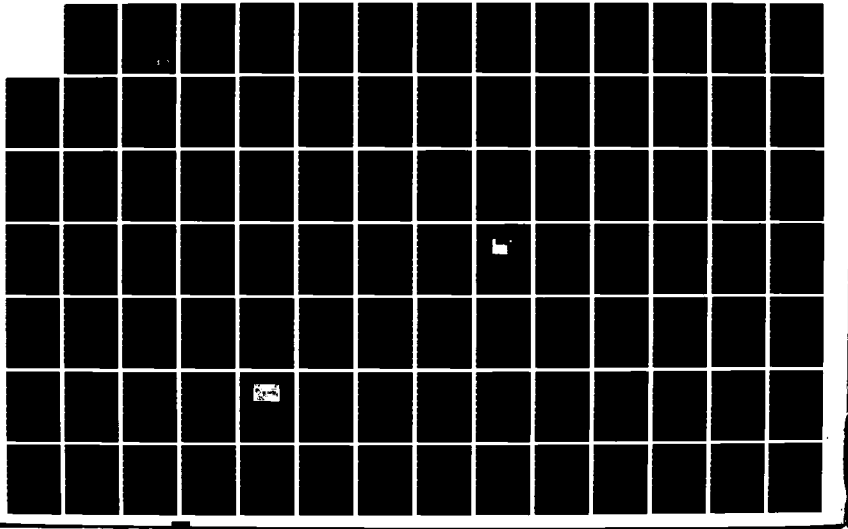

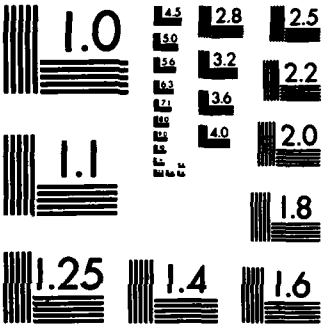

MICROCOPY RESOLUTION TEST CHART
NATIONAL BUREAU OF STANDARDS-1963-A

UNCLASS

SECURITY CLASSIFICATION OF THIS PAGE (When Data Entered)

REPORT DOCUMENTATION PAGE	READ INSTRUCTIONS BEFORE COMPLETING FORM
1. REPORT NUMBER: AFIT/CI/NR 83-34T	2. GOVT ACCESSION NO.: AD-A132 354
	3. RECIPIENT'S CATALOG NUMBER
4. TITLE (and Subtitle): Wear During Rubbing of a Sintered Metal Powder Body	5. TYPE OF REPORT & PERIOD COVERED: THESIS/DISSERTATION
	6. PERFORMING ORG. REPORT NUMBER
7. AUTHOR(s): John R. Rogacki	8. CONTRACT OR GRANT NUMBER(s)
PERFORMING ORGANIZATION NAME AND ADDRESS: AFIT STUDENT AT: University of Washington	10. PROGRAM ELEMENT, PROJECT, TASK AREA & WORK UNIT NUMBERS
11. CONTROLLING OFFICE NAME AND ADDRESS: AFIT/NR, WPAFB OH 45433	12. REPORT DATE: 1983
	13. NUMBER OF PAGES: 102
14. MONITORING AGENCY NAME & ADDRESS (if different from Controlling Office)	15. SECURITY CLASS. (of this report): UNCLASS
	15a. DECLASSIFICATION DOWNGRADING SCHEDULE

16. DISTRIBUTION STATEMENT (of this Report)

APPROVED FOR PUBLIC RELEASE; DISTRIBUTION UNLIMITED

17. DISTRIBUTION STATEMENT (of the abstract entered in Block 20, if different from Report)

18. SUPPLEMENTARY NOTES

APPROVED FOR PUBLIC RELEASE: IAW AFR 190-17

1 SEP 1983

Approved for public release: IAW AFR 190-17.

LYNN E. WOLAVER
Dean for Research and Professional Development
Air Force Institute of Technology (ATC)
Wright-Patterson AFB OH

19. KEY WORDS (Continue on reverse side if necessary and identify by block number)

20. ABSTRACT (Continue on reverse side if necessary and identify by block number)

ATTACHED

DTIC ELECTE SEP 14 1983 S D E

DD FORM 1 JAN 73 1473 EDITION OF 1 NOV 65 IS OBSOLETE

UNCLASS

SECURITY CLASSIFICATION OF THIS PAGE (When Data Entered)

ABSTRACT

Rub interactions were carried out between an abradable nickel-chromium seal material and titanium alloy blades at slow speeds (1,5, and 10 cm/s). Square-ended and negative rake angle blades (-85^{o}) with blade tip lays parallel and perpendicular to rubbing were fed at six different rates ranging from 0.16 to 100 X 10^{-6} m/pass.

When feed was large compared to the blade tip leading edge radius (with square-ended blades), the seal material was cut by the blade. At smaller feeds and with slanted blades, the seal material surface was densified by the blade. Forces increased with incursion at intermediate feeds. At the two smallest feeds, the seal material wore as quickly as it was densified, and so forces leveled off. The effects of changing or stopping feed during a test were also studied. An equation was found which described the decay of forces after feed was stopped and rubbing continued.

The specific energy of seal material displacement increased substantially with feed. A relationship between feed and specific energy of seal material displacement was suggested.

The modulus of elasticity of the seal material was found to vary with strain. Results from tensile tests accomplished during this work were combined with data from compression tests to derive a relationship between modulus of elasticity

and strain.

Based on the results of these tests, it is suggested that the primary mechanism of seal material wear was fatigue.

BIBLIOGRAPHY

L.P.Ludwig,R.C.Bill, "Gas Path Sealing in Turbine Engines", NASA Technical Memorandum 73890 (Revised), 1978.

R.C.Bill,L.P.Ludwig, "Wear of seal Materials Used in Aircraft Propulsion Systems", Paper Presented at the Workshop on Thermal Deformation, Annapolis, Md., 1979.

R.C.Bill,L.T.Shiembob, "Friction and Wear of Sintered Fiber-metal Abradable Seal Materials", NASA TMX-73659, 1977.

J.G.Ferguson, "Use of Coatings in Turbomachinery Gas Path Seals", AGARD Conference Procedings No. 237: Seal Technology in Gas Turbine Engines, 1978.

J.Wolak,A.F.Emery,S.Etemad,S.R.Choi, "Preliminary Results on the Abradability of Porous, Sintered, Seal Material", ASME/ASLE Joint Lubrication Conference, Washington, D.C., Oct. 5-7, 1982, Paper 82-Lub-7.

R.C.Bill,D.W.Wisander, "Friction and Wear of Several Compressor Gas-Path Seal Materials", NASA TP-1128, 1978.

W.F.Laverty, "Compressor Seal Rub Energetics Study Final Report", NASA CR-159424, 1978.

D.H.Buckley, Surface Effects in Adhesion, Friction, Wear, and Lubrication, Elsevier Scientific Publishing Co., New York, 1981.

In presenting this thesis in partial fulfillment of the requirements for a Master's degree at the University of Washington, I agree that the Library shall make its copies freely available for inspection. I further agree that extensive copying of this thesis is allowable only for scholarly purposes, consistent with "fair use" as prescribed in the U.S. Copyright Law. Any other reproduction for any purposes or by any means shall not be allowed without my written permission.

Signature _____

Date _____

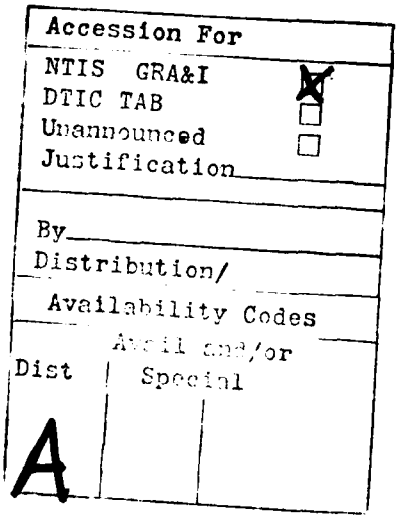

University of Washington

Abstract

Wear During Rubbing of a Sintered Metal Powder Body

By John R Rogacki

Chairperson of the Supervisory Committee: Professor J. Wolak
Department of Mechanical Engineering

Rub interactions were carried out between an abradable nickel-chromium seal material and titanium alloy blades at slow speeds (1, 5 and 10 cm/s). Square-ended and negative 85 degree rake angle blades with blade tip lays parallel and perpendicular to rubbing were fed at six different rates ranging from 0.16 to 100 X 10^{-6} m/pass.

When feed was large compared to the blade tip leading edge radius (with square-ended blades), the seal material was cut by the blade. At smaller feeds and with slanted blades, the seal material surface was densified by the blade. Forces increased with incursion at intermediate feeds. At the two smallest feeds, the seal material was worn as quickly as it was densified, and so forces leveled off. The effects of changing and stopping feed during a test were also studied. An equation was found which described the decay of forces after feed was stopped and

rubbing continued.

The specific energy of seal material displacement increased substantially with feed. A relationship between feed and specific energy of seal material displacement was suggested.

The modulus of elasticity of the seal material was found to vary with strain. Results from tensile tests accomplished during this work were combined with data from compression tests to derive a relationship between modulus of elasticity and strain.

Based on the results of these tests, it is suggested that the primary mechanism of seal material wear was fatigue.

TABLE OF CONTENTS

LIST OF FIGURES

LIST OF TABLES

ACKNOWLEDGEMENTS

The author wishes to express his sincere appreciation to Professor J. Wolak for his tireless assistance and guidance throughout this project. In addition, a special thanks to Mr. Sung Rak Choi and Mr. Robert Zenas for their help during several crucial phases of this work.

CHAPTER I

INTRODUCTION

The demands of rapidly advancing aerospace technology coupled with expectations of increasing energy costs have prompted studies to develop new, more efficient turbine engines. One particularly promising approach to increasing turbine engine efficiency lies in improving the design of gas path seals.

Gas path seal technology has been studied for decades. This chapter briefly reviews the historical background of the design of turbine seals, describes the various types of seals and their functions, examines the impact of rubbing at the blade/seal interface on engine efficiency, and summarizes relevant engine operating conditions. Next is a discussion of desirable seal material characteristics and a survey of four basic types of seal materials that are currently being considered in the search for the ideal seal material. Recent approaches to testing these materials are also discussed.The final section of the chapter outlines the objectives of this work.

Historical Background

As the state of the art in the manufacture of turbine

engines advances, new and better seal materials and designs have been continually sought. Norman L. Mochel (1:p154), in discussing the need for abradable seal materials in steam engines, wrote:

> "Usually one does not ask for rapid wear of parts, but in this case, when rubbing occurs, rapidity of wear is quite desired and necessary. The strip material, because it may be renewed if necessary, must quickly wear away or mushroom, freeing the condition of contact, producing as little local heat as possible, and there must be no tendency to pick up, seize, unduly score or wear the main element, no matter which part it may be."

Mochel further notes that in the early days of steam engine development, Parsons designed seals from a copper/zinc brass mixture for this purpose. These became obsolete, however, as internal temperatures in steam turbines climbed above the mild 700F temperatures of Parson's day to the "scalding" 1050F temperatures that engines in Mochel's time encountered. By way of comparison, aero-engines of the 1980's may operate at internal temperatures in excess of 2500F. Thus, seal technology has had to develop rapidly to meet the demands of modern engines.

Types of Seals and Their Functions

A modern gas turbine engine may have over 50 gas path seals (2). Fig. 1.1 shows the locations, types and functions of seals within a typical engine from a

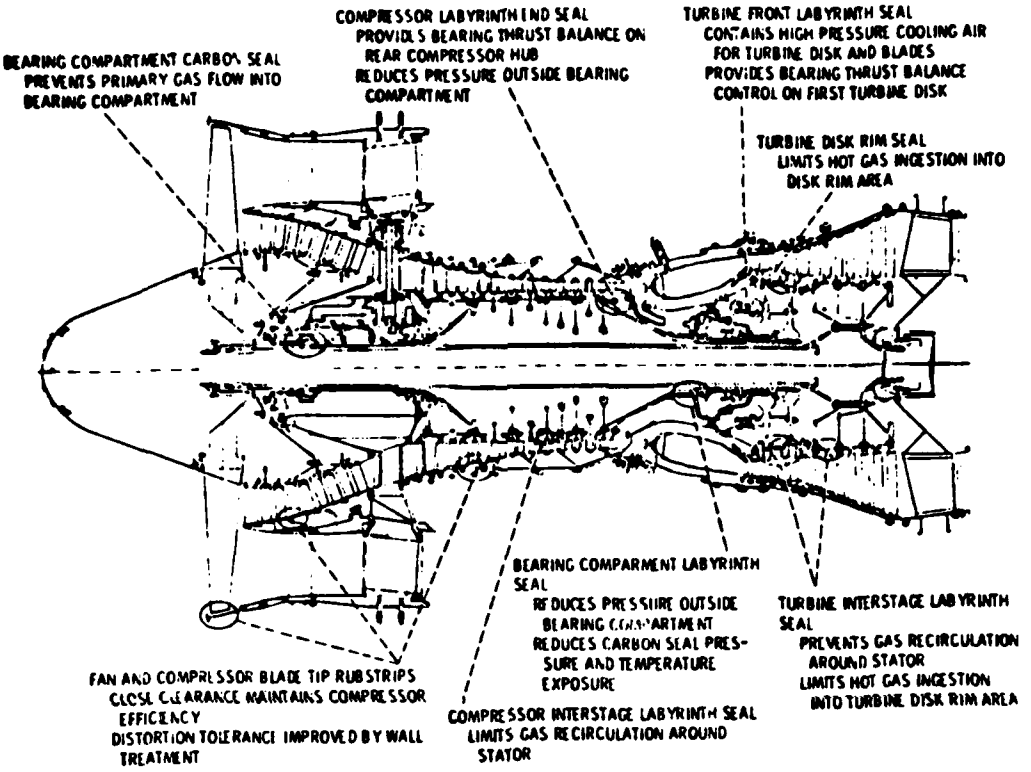

Fig. 1.1 - Seals in a modern transport engine (2).

transport aircraft. According to Bill and Ludwig, two general types of seals are found in turbine engines: mainshaft seals and gas path seals. Mainshaft seals protect the bearing compartment from the potentially damaging environment outside the compartment. These are generally positive contact seals. Gas path seals make up the bulk of turbine seals and fall into two categories: labyrinth and outer gas path (or blade tip) seals. Labyrinth seals reduce the loss of high pressure gas from

the engine, control cooling airflow through the hot section of the engine, and maintain pressure balance on the rotor shaft system. Outer gas path seals, the focal point of this study, reduce pressure losses at the compressor and turbine blade tips. Close operating clearances are maintained between moving blade tips and the stationary seal components, thereby allowing greater engine efficiency (3).

Engine Efficiency vs. Rubbing

Ideally, an engine design should provide minimum operating clearance between blade tips and seal components without any rubbing. A plot of engine efficiency (compressor section in this case) vs. clearance/blade height ratio shown in Fig. 1.2 demonstates the need for close tolerances between blade tips and seal components. Here a small increase in blade clearance (from 1% to 5%) causes an 8% reduction in compressor efficiency (4). In order to improve thrust to weight ratios and to reduce specific fuel consumption, modern engines are constructed of lighter weight components than ever before. This usually means a more flexible structure and a greater susceptibility to aerodynamic excitations. The combination of increased flexibility and reduced blade tip clearances may result in rubbing between blade tips and seal materials (5:p221).

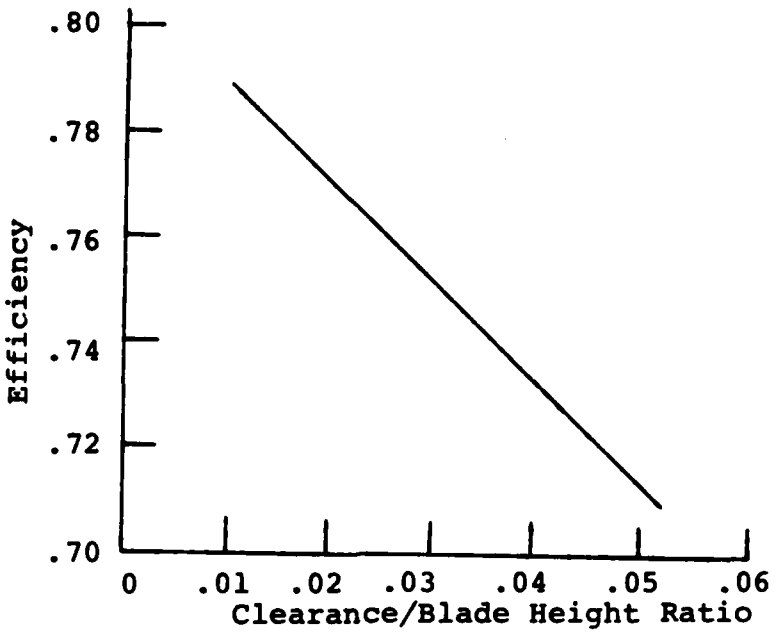

Fig. 1.2 - Compressor efficiency as a function of Clearance/Blade Height ratio (4).

According to Bill and Ludwig, other factors leading to rubbing may also include:

- thermal response of the casing and rotor;
- centrifugal and gyroscopic loads;
- surge/stall displacements;
- thrust, aerodynamic, gust, maneuver and landing loads;
- out of roundness;
- assembly eccentricities;
- machine tolerance variations (2).

Fig. 1.3 illustrates the potential for rubbing between engine case (or seal component) and rotor (or rotating

blades) during typical engine operating conditions.

Rubbing, therefore, is inevitable in any engine which is designed to have reasonably close clearances between blade tips and seals. Unfortunately, the immediate effect of this rubbing is a reduction in the engine efficiency that was sought to begin with.

Fig. 1.4 is a simplified illustration of what happens when rubbing occurs: in the first case, the blades wear, and in the second, the seal material wears. For simplicity, the rotating blades are depicted as a solid disk, and the clearance is greatly exaggerated. In both cases, there is an increase in flow area around the blade tips which allows gas (and energy) to escape, but this problem is more severe when the blades wear. Moreover, in the first case there is also a decrease in total blade area and a possible loss of efficiency across the entire blade if the aerodynamic characteristics of the blade are altered (2). Clearly, then, it is desirable to have the seal material wear instead of the blades, and seal abradability becomes an important factor in seal material selection. Several environmental factors, however, complicate the selection process.

Effect of Operating Environment on Seal Material Selection

The operating environment within a turbine engine is extremely varied, making seal material selection

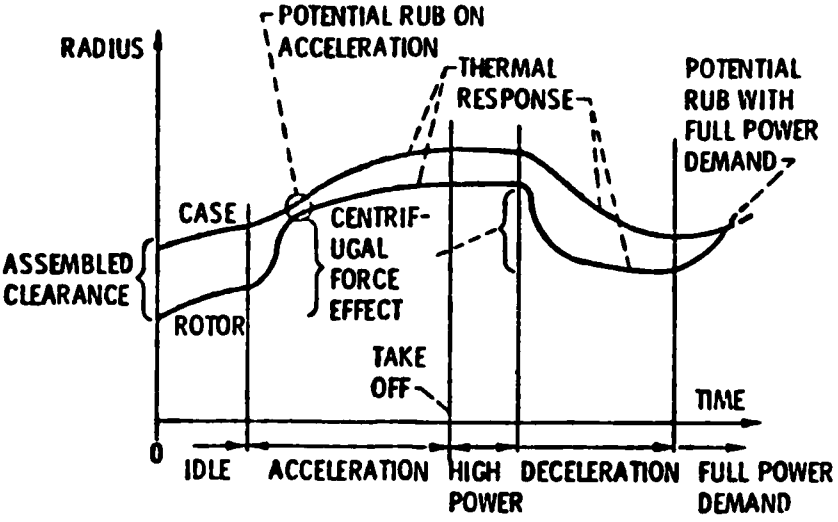

Fig. 1.3 Change in clearance between casing and rotor during typical engine flight profile (2).

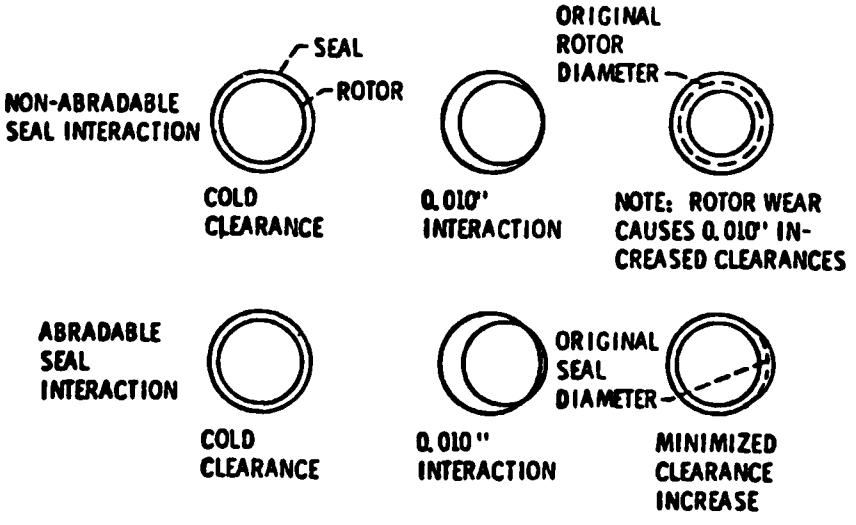

Fig. 1.4 - Non-abradable (top) and abradable (bottom) seal interaction. Clearance is more adversely affected in non-abradable interaction (3).

difficult. Temperatures in turbine engines range from ambient (as low as -50F) to above 2500F, so different materials are used in different sections of the engine. For example, Rolls Royce has used resins and rubbers for fan and low pressure compressor seals, but they selected flame sprayed nickel/aluminum and nickel chrome/aluminum for high pressure turbine tip seals (7). The most adverse environment is found in the high pressure turbine section where temperatures up to 2600F and pressures up to 25 times atmospheric may be encountered (2).

Another serious problem is erosion, which can be caused by airborne dust or debris, or perhaps by particles generated by a seal rub upstream in the engine. Since these particles travel at extremely high speeds, they can produce high erosion rates. Seal materials, therefore, must be erosion resistant, or the seals will wear prematurely, resulting in a decrease in engine efficiency. Unfortunately, erosion resistance requires high cohesive strength - a property which tends to increase blade wear when rubbing takes place (6).

Other desirable seal material properties include stability in an oxidizing atmosphere, resistance to thermal shock, impact resistance, and dimensional stability in a volatile environment (8). Unfortunately, most materials which satisfy these requirements are strong and hard enough to cause blade wear when the blades

contact the seals. This, as previously mentioned, impacts unfavorably on engine efficiency and fuel consumption.

Materials Under Consideration for Use in Seals

At least four basic types of materials have been studied recently as solutions to the gas path seal dilemma. These include high porosity, low density materials, denser (less than 30% porosity) plastically deformable materials, honeycombed metal alloys, and various forms of ceramics. Each is briefly discussed below.

High Porosity, Low Density

This group includes sintered metal powders or fiber particles mixed with transient filler materials and plasma sprayed metal particles mixed with easily volatizable polymeric particles or with graphite. The material used in this study was a sintered powder of an alloy of 80% Ni and 20% Cr. In theory, abradability in this group is high because fracture readily occurs across the small bonds between particles in the seal when the blade comes in contact with them. Discrete particles are thereby removed from the seal material, reducing frictional heating and wear to the blades.

Problems associated with low density, high porosity materials include susceptibility to erosion and

inefficient sealing through open pores. Furthermore, rub interactions may lead to smearing, which increases the density of the material. As the density increases, subsequent wear to the blade tip also generally increases (9). Fig. 1.5 is a simplified illustration of the rubbing interaction between a blade and seal with and without smearing (10).

Although the exact mechanism responsible for the onset of smearing and the consequent rapid frictional heating and wear is unknown, several explanations have been offered, but none has proven to be completely satisfactory. This will be addressed in considerable detail in Chapter IV.

Dense, Plastically Deformable Materials

These materials are denser than those of the first group and may be plasma sprayed, sintered, hot pressed, or even cast. Bill and Wisander estimate that these materials accomodate rubbing by a combination of plastic deformation, material compliance (densification) and machining mechanisms (10). The radial or normal load, according to Bill and Wisander, is controlled by plastic indentation considerations, and the frictional energy resulting from the rub is then the product of this normal load, the coefficient of friction and the rub velocity. As with the first group of materials, blade penetration can

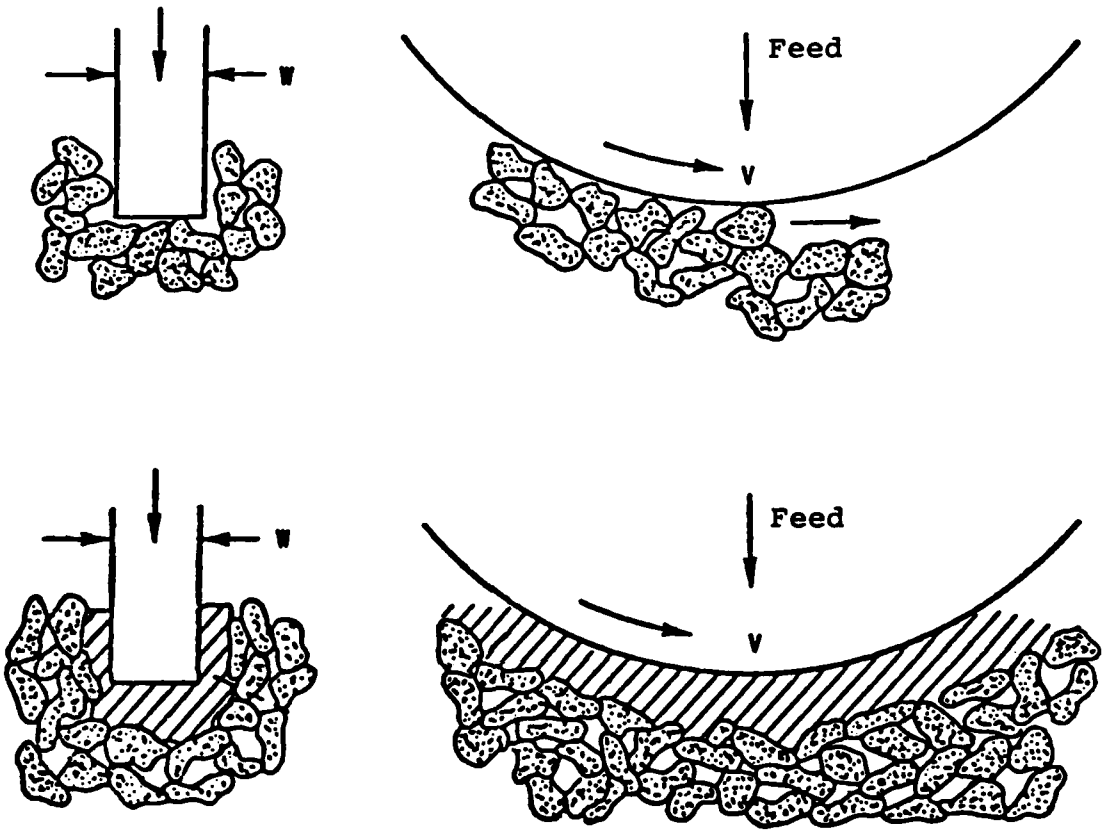

Fig. 1.5 - Interaction between blade and seal showing abradable interaction (top) and smearing (bottom) (10).

cause densification and increase rub intensity, heating, blade wear, etc.

Honeycombed Metal Alloys

The third group of proposed seal materials consists of honeycomb structured metal alloys. The honeycomb cell walls are oriented radially around the engine casing. This results in less metal to metal contact surface area when a rub occurs.

Honeycomb materials offer better oxidation resistance than lower density materials and are more abradable than the denser structures. Because of their rough surface, however, honeycomb seals are less efficient aerodynamically than other types of seal materials. A further disadvantage of the honeycomb structure is the pressure leakage loss suffered through the open face structure. These properties make honeycomb materials suitable for use at high temperatures but unsuitable for high pressure locations in the engine (3). For these reasons, honeycomb materials are generally used in low pressure turbine locations, as well as in the fan section of some engines (7).

Ceramic Materials

Various ceramic materials and structures have been considered for use in seal applications. Ceramics, of

course, are noted for their excellent high temperature properties, oxidation resistance, relative abundance and low cost. Moreover, because of their brittle nature, ceramics have a lower tendency to smear than metals. Drawbacks include possible susceptibility to thermal shock and low impact resistance.

Vogan et al (8) evaluated silicon nitride and silicon carbide in compacted and honeycomb forms. The SiN honeycomb structure exhibited some potential for use as a seal material, displaying such desirable characteristics as clean fracture of seal particles, virtually no blade wear, and good oxidation resistance. However, such factors as fatigue resistance, susceptibility to thermal shock, and permeability to hot gases in a high pressure environment were not discussed.

Recent Approaches to Testing of Seal Materials

Numerous tests have been run studying the behavior of seal materials. Two basic approaches have been employed. The first, used by Laverty (11), had stationary blades rubbing against seal materials bonded to rotating test disks (Fig. 1.6). Incursion rates ranged from 0.0025 mm/sec to 0.25 mm/sec and rub velocities from 152 m/sec to 213 m/sec.

Laverty recorded rub torque, speed, incursion rate and blade temperature while varying rub depth, incursion

rate, abradable density, blade thickness and velocity to simulate engine compressor rubbing conditions. He encountered three distinct rub modes:

1. a low energy, low blade wear mode occuring at low incursion rates;
2. transfer of seal material to the blade tips when moderate and high incursion rates were used;
3. a high rub energy, high wear rate rub mode under the combination of high incursion rate, low rub velocity and thick blades.

The most influential variable, according to Laverty, was incursion rate.

The second testing approach, used by most other researchers, utilizes a rotating blade or series of blades against which a sample of seal material is fed at varying rates (Fig 1.7). Information obtained from this type of apparatus includes frictional and normal forces, thermal effects, wear of the seal and blade surfaces, material transfer and seal abradability. Test conditions used by Wolak et al (9), typical of those used by others in this approach, include incursion rates of 0.0125 mm/s and 0.025 mm/s and a rubbing velocity of 100 m/s.

Objectives of This Work

Despite the tremendous amount of resources expended

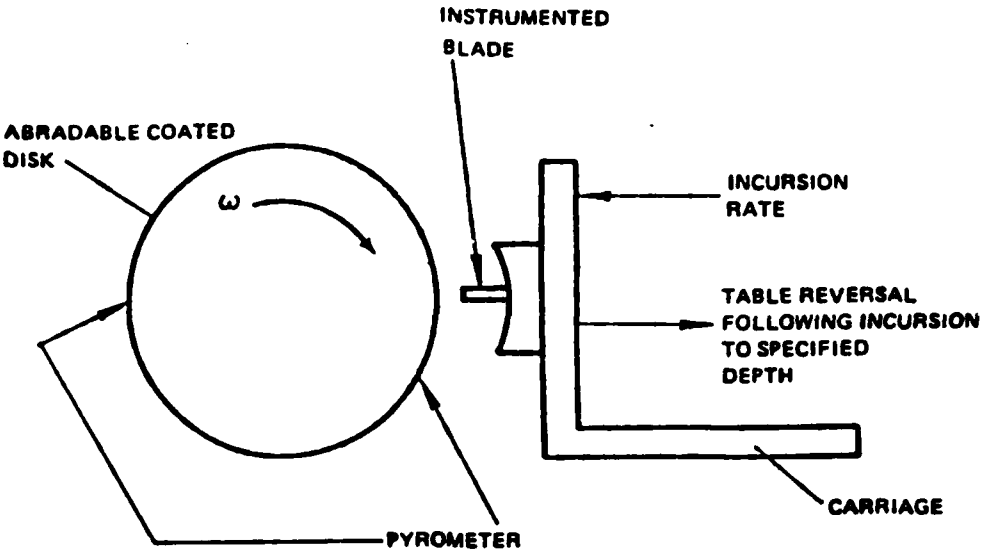

Fig. 1.6 - Rub test apparatus used by Laverty (11). Blade is fed against disk coated with abradable seal material.

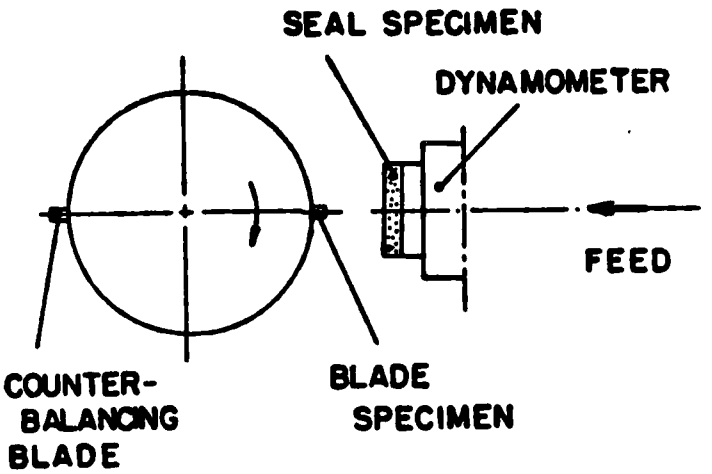

Fig. 1.7 - Rub test apparatus used by Wolak (12). Seal specimen is fed against rotating blade specimen.

in studying the blade/seal rubbing interaction, much remains to be learned. The exact mechanism of material removal is still an object of speculation, and the effects of various factors such as blade geometry, incursion rate, etc. are not well understood.

In an attempt to achieve a better understanding of the blade/seal interaction, this study focuses on low speed rubbing between Ti-6-Al blades and a porous sintered nickel-chromium seal material. Studying the rub interaction at low speed provides two advantages. First, the rub interaction can be observed and photographed. This has not been possible to date using high speed rub testers. Second, data obtained from these low speed tests can be compared with published results from the high speed tests. Similarities and differences between the two would then provide some insight into the rubbing process.

CHAPTER II

EXPERIMENTAL APPARATUS FOR RUB TESTING

In order to better understand the rubbing interaction between turbine blades and gas path seal materials, a low speed apparatus was developed which would facilitate recording the interaction photographically and also provide data to compare with the high speed data obtained in other studies. This study focuses on the effects of various parameters on rubbing forces, both normal (Fn) and tangential (Ft), and seal densification factor (Sd). The parameters studied include cutting speed (Vc), feed (f), and blade geometry, including rake angle and blade tip lay. This chapter describes the materials and equipment used in the experiment.

Blades

Blade specimens were made from Ti-6Al-4V material, similar to those found in turbine engines. It was found from high speed tests that blade tip geometry has a significant impact on rub performance (9), so two different blade tip geometries were used: one with a negative rake angle of 85 degrees, and the other square ended (see Fig. 2.1). Each blade was mounted in a jig and ground on a vertical grinder before being used in a rub

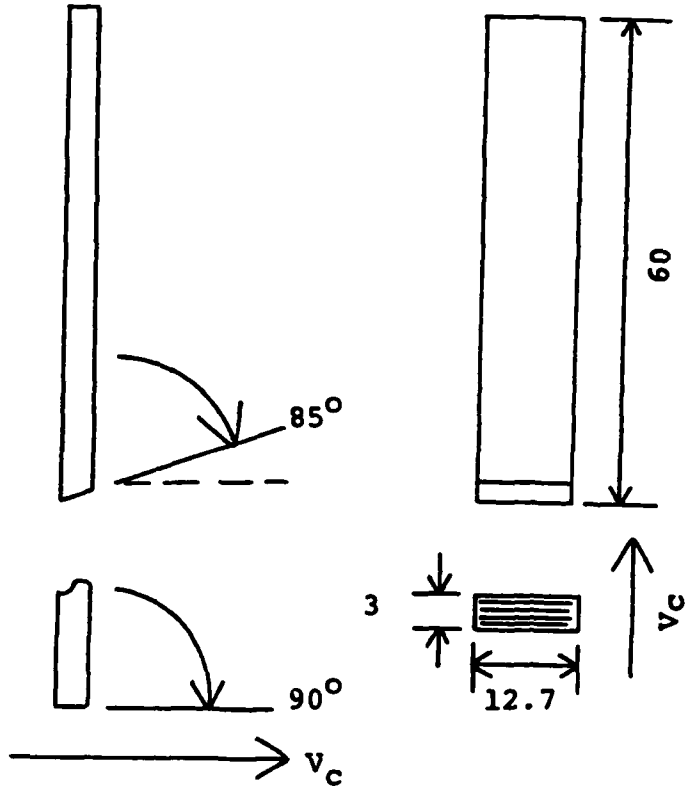

Fig 2.1 - Blade specimen with negative rake angle of 85° (upper left) and 90° (lower left). Blade tip shown at lower right has lay perpendicular to rubbing direction. All dimensions are in millimeters.

test. During blade preparation, the blade tips were ground either perpendicular or parallel to the rub test cutting direction (Fig 2.1). This permitted a study of the effect of blade tip lay on the rubbing interaction.

Seals

The seal material used in this experiment was a sintered powder of 80% nickel 20% chromium alloy, 40% dense, meeting P&WA Spec No.1090-2. All seal specimens

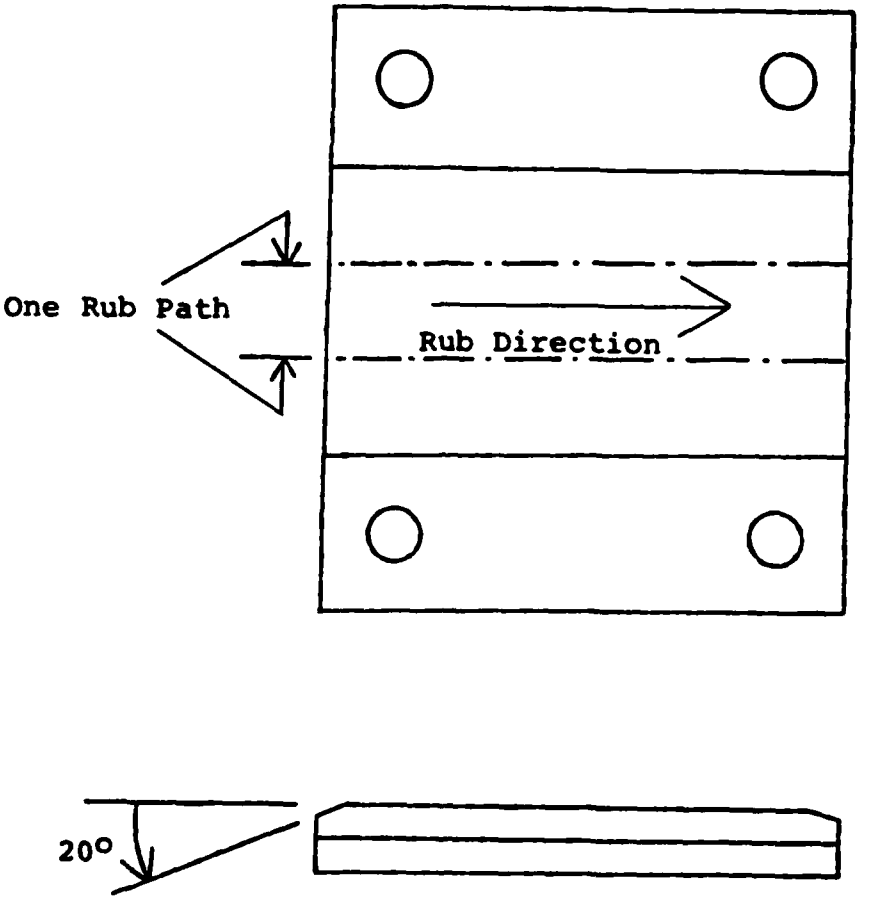

Fig. 2.2-Typical seal specimen used during rub testing. Rub path shown is center path of three on each specimen.

were approximately 38mm wide by 63mm long. Seal specimens #1 through #10 were mounted on 3.2mm thick aluminum plates using a thin (less than 1mm) coat of epoxy. Seal specimen #11 was soldered to a 1.6mm thick steel plate. The use of solder in place of epoxy permitted the specimen to be thoroughly cleaned in acetone prior to and during testing. The ends of the specimens were chamfered to 20 degrees to the horizontal (Fig. 2.2) on a milling machine to reduce the impact forces at the initiation of each rubbing pass.

Test Bed Characteristics

Several special testing machines have been constructed by other researchers in order to study the parameters which affect the blade/seal rubbing interaction. These machines all operate at high speeds to simulate turbine rubbing conditions. In order to evaluate and photograph the interaction at low speeds, a suitable testing apparatus had to be developed.

The following characteristics were considered especially important in selecting a test bed for this experiment. First, a feed rate of 2.5×10^{-6} m (0.0001 inch) per pass or less had to be attainable. This amount is far less than usually required in machining operations. Next, compatibility with available photographic and force measuring equipment was evaluated. For example, a very slow cutting speed (Vc = 1cm/sec) was eventually utilized

when attempting to photograph the rubbing process. In addition, several pieces of equipment (e.g. dynamometers, camera, etc.) would have to be located on or in the immediate vicinity of the test bed. Finally, a rigid and stable test bed was required to reduce errors caused by loads encountered during rubbing.

Rockford Planer

A Rockford planer was found to most nearly satisfy all of the desired test bed characteristics, but several problems had to be overcome before testing began. The problem areas were minimum attainable feed increment and test bed rigidity. The problems and their solutions are discussed below. After several modifications were made, the planer performed satisfactorily as a test bed throughout the rub tests.

Feed Increment

In order to simulate incursion rates encountered in actual blade/seal rubbing interactions, feed increments of 2.5×10^{-6} m/pass or less are necessary. The feed mechanism supplied with the planer moves the clapper head (and attached tool) 5000×10^{-6} m/revolution of the crank handle. Furthermore, because of the gearing between the crank handle and clapper head, the handle is difficult to turn in small increments. These two factors make the

minimum feed increment using the existing mechanism about ten times the desired amount. In addition, a backlash of 75 to 100 X 10^{-6} m was discovered when a relatively small normal force was applied to a cutting tool mounted in the clapper head. For these reasons, the original feed mechanism was deemed inadequate for this experiment, and a modification was necessary.

A new feed mechanism was designed which could control feed in increments less than 2.5 X 10^{-6} m/pass. The mechanism utilizes a lever arm with one arm attached to the clapper head screw (Fig. 2.3). The opposite end of the lever arm has a nut mounted in it through which a long feed screw is passed. The spherical end of the feed screw is attached to a fixture on the planer crossarm. The screw is free to rotate, but cannot move longitudinally. As the screw turns inside the lever arm, it causes the lever arm to turn the clapper head screw. Turning the clapper head screw lowers the cutting tool. One 360 degree revolution of the feed screw, for example, causes the lever arm to rotate 0.18 degrees, which lowers the cutting tool 2.5 X 10^{-6}m. Backlash, an important consideration at such small feeds, is discussed later in this chapter under the heading "Gear Backlash".

Machine Deflections Under Loading Conditions

Since it is essential that the motion of the test bed

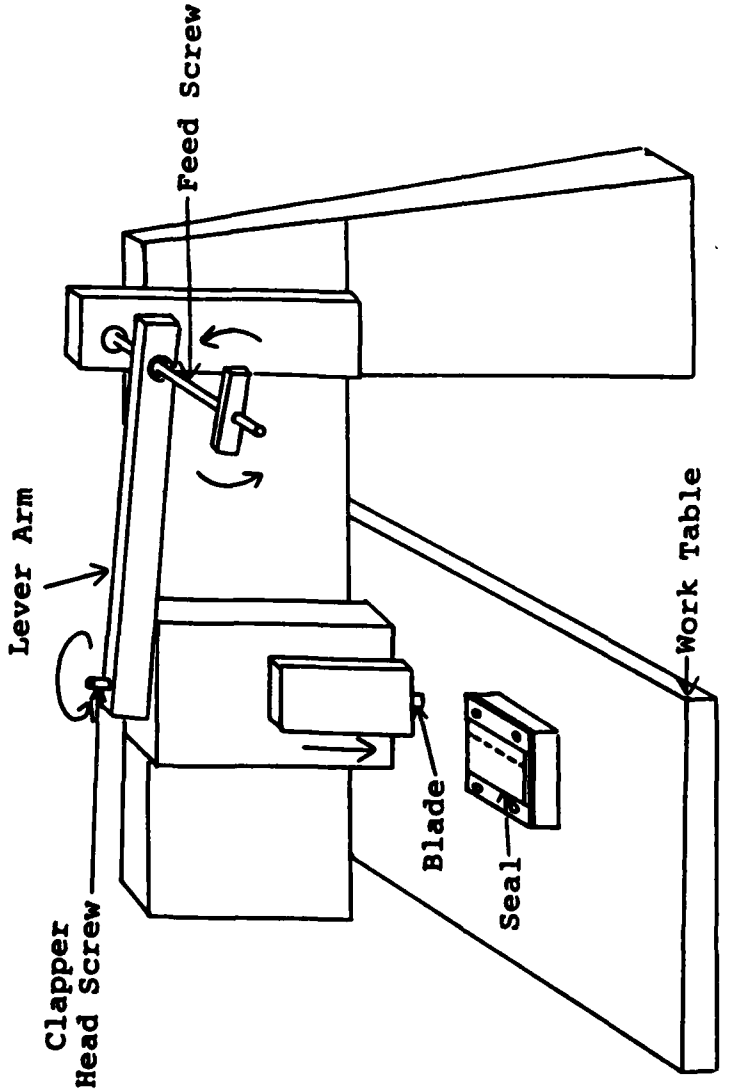

Fig 2.3 - Feed mechanism. When the feed screw is rotated, the lever arm turns the clapper head screw, which lowers the blade.

be repeatable and that the amount of error introduced into the data be minimized, the planer was checked for stability during operation. Through use of a proximitor attached to the clapper head, the planer table was checked for vibrations and other undesirable vertical movement. No vibrations were detected (proximitor discrimination $< 2.5 \times 10^{-6}$ m). The maximum relative vertical movement between the proximitor and the surface passing under it (a polished dynamometer) was $< 4.0 \times 10^{-6}$ m. This movement was repeated on every pass, and was probably due to a slight taper in the dynamometer surface. These errors were considered to be insignificant.

An initial check of the relative movement under load between the clapper head (or cutting tool) and table top (or workpiece) yielded unacceptable results. The clapper head moved more than 100×10^{-6} m under a load of 890N and 40×10^{-6} m with a load of 445N. These amounts are obviously incompatble with the desired feed increment of 2.5×10^{-6} m.

A check of the pin connecting the clapper head to the crossarm assembly revealed a combination of eccentricities which could potentially account for up to 125×10^{-6} m movement. The pin was subsequently ground and lapped to fit more precisely into the crossarm assembly and another check was made for relative movement. The movement was reduced to 6.25×10^{-6} m at 445N. This movement was then

further analyzed by applying the load on different components and checking the deflection of each. The following results were obtained:

- with the load applied directly to the table top, dy = 1.25 X 10^{-6}m at 445N and 2.5 X 10^{-6}m at 890N (Figs.2.4a,2.5a);
- when the load was applied to the crossarm, dy = 4.00 X 10^{-6}m at 445N and 10.25 X 10^{-6}m at 890N (Figs. 2.4b,2.5b);
- with the load applied to the clapper head, dy = 16.0 X 10^{-6}m at 890N (Figs. 2.4c,2.5c).
- with the load applied to the clapper head, the total deflection between the clapper head and the table top was 6.25 X 10^{-6}m at 445N and 21.3 X 10^{-6}m at 890N (Fig.2.5d);
- the movement between the clapper head and the crossarm assembly was zero up to 675N, and dy = 8.75 X 10^{-6}m at 890N (Fig 2.4d);
- the movement between the clapper head and table top was almost perfectly linear with respect to force up to 675N (Fig 2.5d).

Based on these results, the relative movement of the clapper head with respect to the table top was considered acceptable for normal forces up to approximately 675N. A correction could be made, if deemed necessary, to the depth of cut values based on the linear relationship

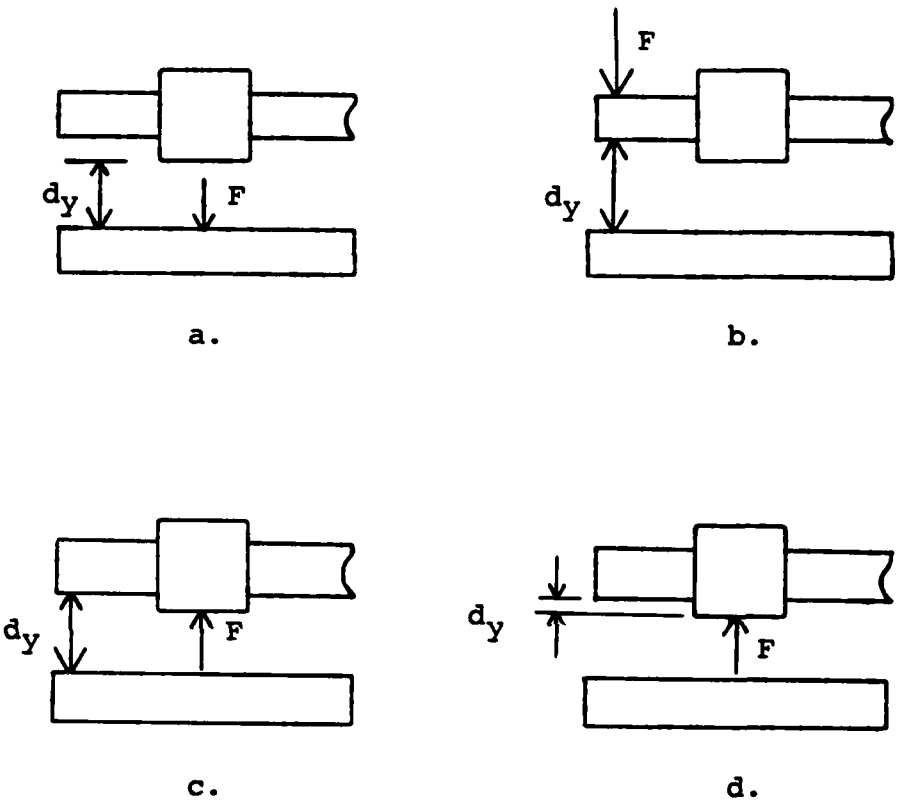

Fig. 2.4a-d. Machine deflections under loading conditions.

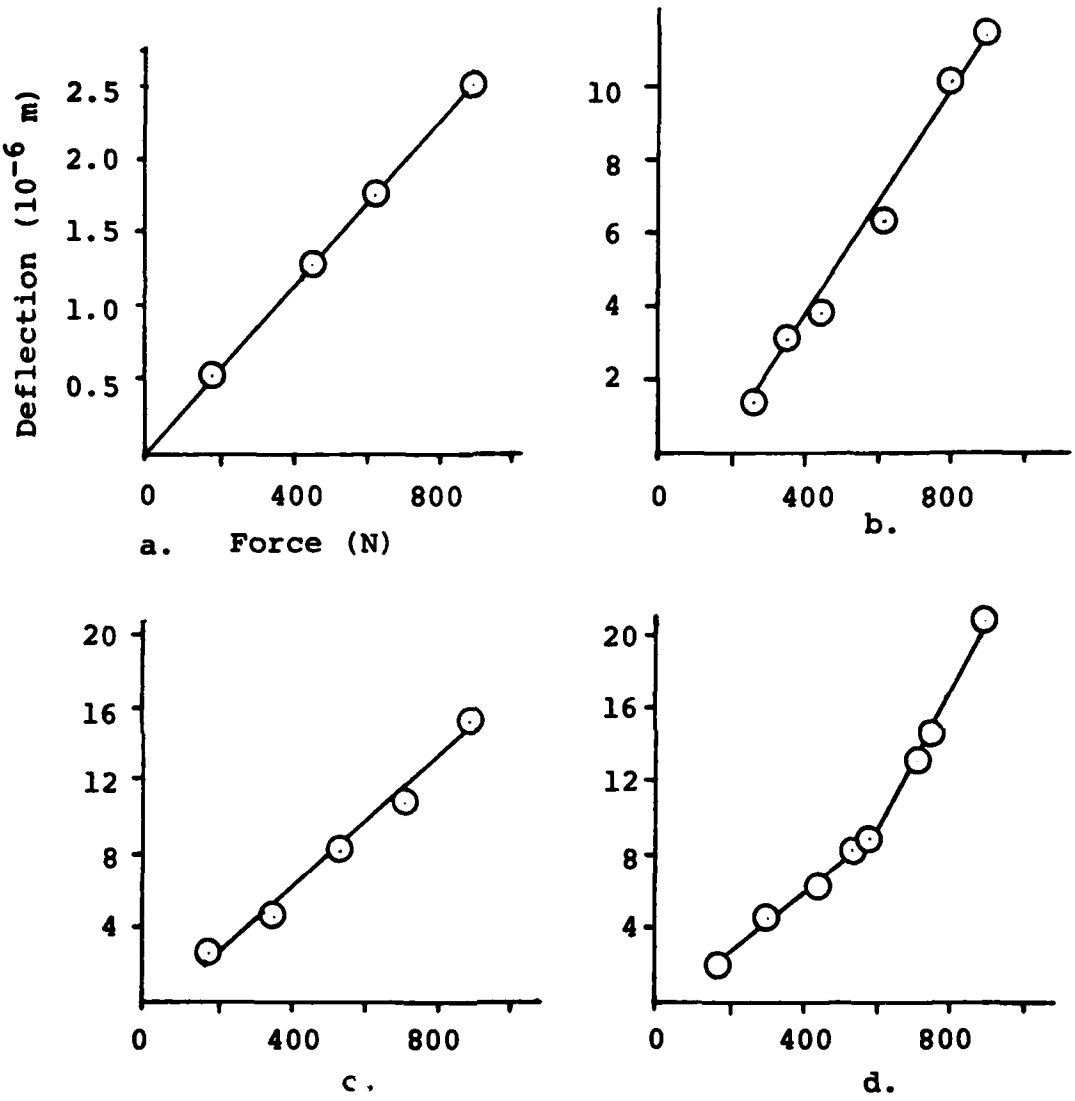

Fig. 2.5a-d: Machine deflections under various loading conditions.

between movement and normal force noted above. Above 675N, an inaccuracy in the feed increment would be introduced by clapper head movement.

Gear Backlash

The new feed mechanism bypassed all but one gear between the feed screw and the clapper head, so most of the backlash problem was eliminated coincidentally. In order to eliminate the backlash from the remaining gear, a force of 1335N was applied to the clapper head opposite to the force Fn through use of a lever arm and weights (Fig 2.6).

Clapper Head Rotation

The planer worktable moves with a reciprocating motion on a horizontal line beneath the cutting tool. Between cutting strokes (on the backstroke) the clapper head rotates to allow the workpiece to move beneath the cutting tool without contacting the tool. In order to ensure that the clapper head returned to the same position before each pass, an 11 kg weight was mounted onto the clapper head (Fig. 2.7).

Force Measuring Equipment

Two dynamometers recorded the forces encountered during rubbing. The first, a Kistler piezo-electric

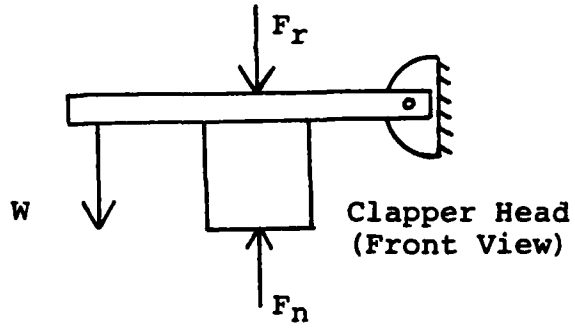

Fig 2.6 - Lever and weights added to eliminate gear backlash. F_r is the resultant force on the clapper head due to the addition of weight, W. F_n is the normal force due to rubbing.

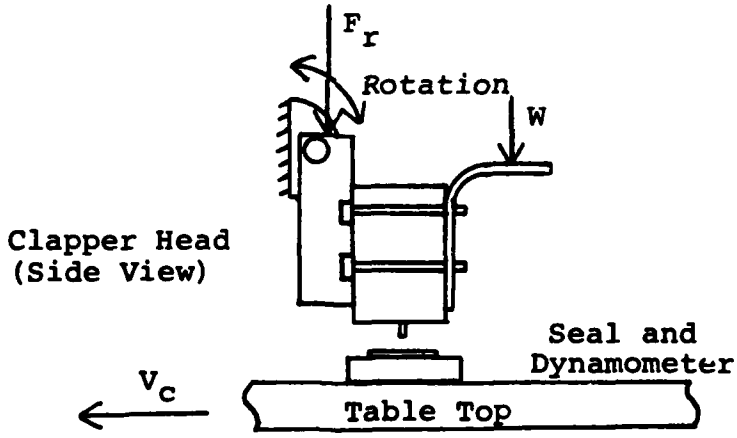

Fig 2.7 - Clapper head rotation. Weight (W) was added to insure that the clapper head returned to its original position after each pass.

dynamometer, type 9257A, was mounted directly on the planer table. The seal specimen was then bolted to the dynamometer. The other dynamometer, a strain gage type deigned by Prof. J. Wolak of the Mechanical Engineering Department, University of Washington, was attached to the planer clapper head. The blade specimen was then mounted onto this dynamometer. Since both dynamometers measured the same forces (dynamical effects ignored), they provided a good crosscheck for one another.

Kistler charge amplifiers (models S/N 506 and 504A) were used with the piezo-electric dynamometer, and Vishay (model 2310) amplifiers with the strain gage dynamometer. A Gould Brush 440 four channel oscillograph recorded the rubbing forces.

Photographic Equipment

Movies of the rub interaction were taken with a 16mm camera using a 3 inch lens and 38mm extension tube. Lighting was provided by two Colortran high intensity lamps, each approximately 2.5m from the blade tip. This allowed for a film speed of 64 frames/sec at F5.6. The cutting speed during all photographs was 0.3m/min. Kodak Tri-X Reversal film was used (daylight ASA = 200).

Still pictures were taken of the blade tip and seal material at various depths of incursion during tests #27 and 28 using a 35mm camera equipped with a nest of three

close-up lenses. The lenses, when used in series, provided a magnification of +7 diopters. Kodak Tri-X film with an ASA of 400 was used.

CHAPTER III

EXPERIMENTAL PROCEDURE

After making the necessary modifications to the Rockford planer (Chapter II) and assembling and calibrating the force measuring equipment (Chapter II and Appendix A), the actual rub testing procedure was initiated. The rub testing procedure consisted of three phases: preparatory, test and post-test. In addition, tensile tests were performed on the seal material. These tests are described seperately below.

Preparatory Phase

During the preparatory phase, the equipment was readied and preliminary data gathered. The blade and seal specimens were weighed using a Mettler balance (Type P 162) accurate to 0.001 grams and having a total weight capacity of 160 grams. Because the seal material supplied by the manufacturer was not uniformly thick (differences of up to 0.125mm on an individual specimen and 0.5mm between specimens), each seal specimen had to be measured with a micrometer prior to rubbing in order to determine its initial thickness and volume. The seal specimen was then bolted to the Kistler dynamometer (already mounted on the planer table) with four flathead screws and the blade

inserted into an adaptor in the strain gage dynamometer (previously mounted to the clapper head). Four set screws were used to clamp the blade in place in the adaptor and thus prevent slipping.

Once the blade and seal specimens were in place, an initial adjustment was made to the clapper head to visually position the blade tip approximately 0.025mm from the top surface of the seal. For the sake of convenience, the original feed mechanism was used to make the initial adjustment. This was done by loosening the bolts which clamp the lever arm to the clapper head screw, thus bypassing the new feed mechanism and allowing the clapper head screw to rotate freely as the crank handle is turned. Having set the initial clearance, a dial indicator (0.0025mm accuracy) was inserted between the clapper head and the table top to check for movement as the lever arm was reclamped onto the clapper head screw. The dial indicator was then removed before the table was set in motion.

The electronic force measuring equipment was turned on 30 minutes to 1 hour prior to the start of rub testing to insure adequate warm up time. Equipment settings used during calibration and all rub tests are shown in Table 3.1.

The desired cutting speed was set by adjusting a metering valve on the planer and checked with a stopwatch

(accuracy 0.1 seconds) prior to and during rubbing.

Instrument	Settings
Kistler Ch Amp 506 (Ft)	Sensitivity: 0.5mV/pc Calibration Constant: 7.90pc/N
Kistler Ch Amp 504A (Fn)	Sensitivity: 500N/V Calibration Constant: 3.72pc/N
Vishay Amp 2310 (Fn, Ft)	Gain: 2500 Excitation Voltage: 2.0
Gould Oscillograph	Sensitivity: As Required

Table 3.1 - Force measuring equipment settings.

Test Phase

Once the electronic equipment was warmed up, the preliminary measurements taken, the specimens secured in place, and the cutting speed set, the rub testing began. Compressed air was directed downstream of the blade/seal contact area to remove wear debris from the seal specimen between rubbing passes during tests #1 through 23. Wear debris was vacuumed between passes during tests #26 through 28. The blade was fed in increments of 12.5×10^{-6} m/pass or less (not to exceed the feed increment to be used during the actual test) until contact was indicated by a deflection on the chart recorder. The blade was then fed at the desired feed increment, and the normal and

tangential forces were continuously recorded. Total feed for each rub test was 0.63 to 0.75mm. However, because of mechanical limitations, the new feed mechanism had to be reset after approximately 0.25mm incursion, so the total depth of incursion was accomplished in three segments of about 0.25mm feed each.

Between segments, the seal specimen was removed from the dynamometer and the thickness was measured with a micrometer to insure that the feed was accurate. Meanwhile, the bolts clamping the lever arm to the clapper head screw were loosened and the lever arm was reset by rotating clockwise. The seal was then remounted and the blade repositioned near the seal using the procedure outlined in the preparatory phase. Once this was accomplished, the lever arm was reclamped to the clapper head screw and the next segment of the rub test was begun.

During tests #27 and 28, photographs were taken of the blade tip and seal material at various incursions to record blade wear and smearing on the surface of the seal.

Post-Test Phase

Upon completion of the test phase, the seal and blade specimens were removed and weighed. The seal specimen was again measured with a micrometer to establish the total depth of material removed/densified. This measurement, along with the initial thickness measurement and the

initial and final weights, was used to calculate the change in seal volume, the blade to seal wear ratio, and the seal densification factor. Sample calculations are shown in Appendix II.

Photographs of the blade tip, taken during tests #27 and 28 (see Fig. 3.1), were developed and then examined under a microscope. An optical comparator was used to estimate the width of wear on the blade tip. Since the rake angle of the blade was known (-85 degrees), the change in blade length due to wear (K) could be calculated from the blade geometry:

$$K = \text{wear width} \times \arctan(85^{o})$$

Experimental Variables

The parameters studied during these tests include cutting speed, feed, and blade geometry. The specific values used in each test are summarized in Table 3.2. Cutting speeds used during the tests were 1, 5, and 10 cm/sec. Feed rates were 0.16, 0.625, 2.5, 12.5, 50.0, and 100.0×10^{-6} m/pass. Two negative rake angles, 90 and 85 degrees, and two blade tip surface lays, parallel and perpendicular to the cutting direction, were used.

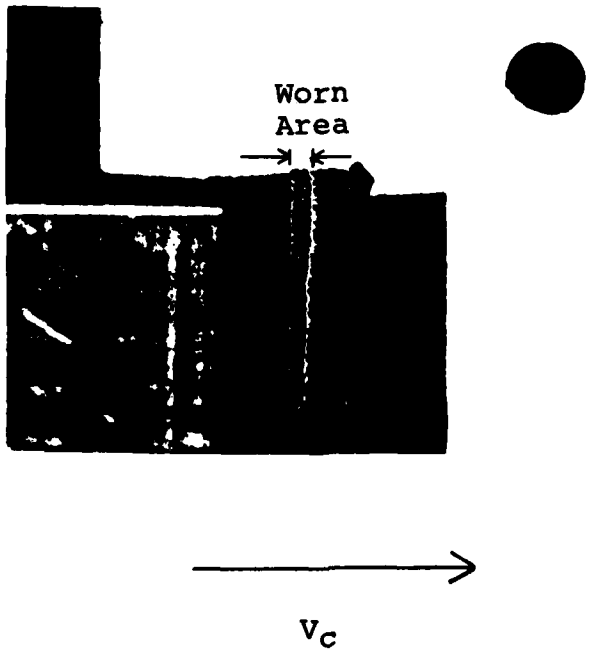

Fig 3.1 - View of blade tip showing wear midway through test #28. Photo was taken looking up at the bottom of the strain gage dynamometer and adaptor.

Test #	Neg. Rake Angle	Vc (cm/sec)	Feed (10^{-6} m)	Blade Lay*
7	90	1	12.5	2
8	90	5	12.5	2
9	90	10	12.5	2
10	85	5	12.5	1
11	90	5	2.5	2
19	90	1	50.0	2
20	90	1	100.0	2
21	85	1	50.0	2
22	85	1	100.0	1
23	85	1	100.0	2
26	85	5	variable	2
27	85	5	variable	2
28	85	5	variable	2

* Blade Lay: 1 = parallel to rubbing, 2 = perpendicular to rubbing direction.

Table 3.2 - Experimental data for rub tests.

Tensile Test

The compressive properties of the sintered porous seal material used in this test had previously been investigated by Wolak et al (9), but the tensile properties had not. Therefore, in order to understand the tensile properties of the seal material (i.e. stress-strain relation, modulus of elasticity, etc.), two tensile tests were performed. Specimens were machined according to ASTM standards (13:p208) for sheet-type tension test specimens (standard and substandard size).

The substandard size specimens were carefully milled to the proper size and shape on a vertical milling machine. The standard size specimens were cut using a

thin, high pitch blade on a band saw at extremely low feed to prevent smearing. Irregularities on the standard size specimen were gently filed from the surface. Dimensions of the specimens are shown in Fig. 3.2.

Because the material is highly porous and relatively fragile, the ends could be susceptible to crushing or premature fracture when mounted in the grips of the Instron testing machine (Model TTCML). To alleviate this problem, the specimen ends were permeated with "Cold Cure", a very wet marine-type epoxy. The epoxy increased the toughness of the grip sections without affecting the material within the gage length.

During the tensile tests, strain was measured with an Instron strain gage extensometer, type G-51-11, and load vs. displacement data was recorded by the Instron X-Y Chart Drive System. Crosshead speed was 0.05mm/sec for the substandard size specimen and 0.005mm/sec for the standard size specimen. Results are shown in Chapter V.

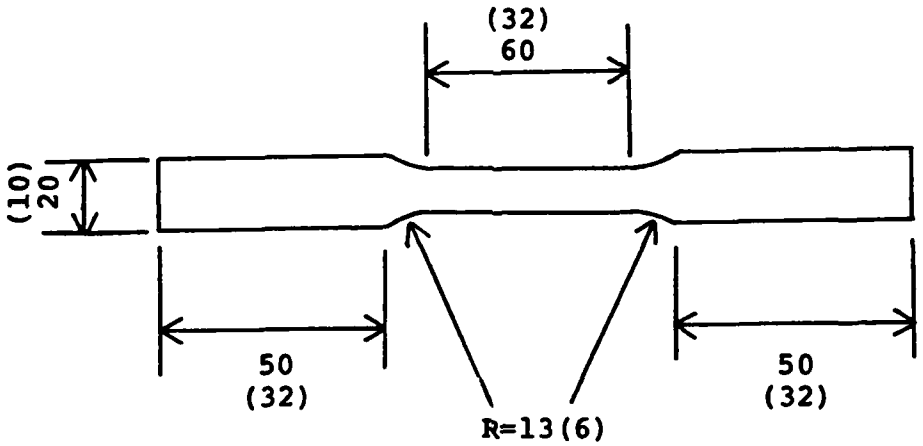

Fig. 3.2-Tensile test specimen. Numbers in parentheses are dimensions of Subsize specimen. Non-parenthesized numbers are dimensions of Standard specimen. All dimensions shown are in millemeters. R is the radius of the fillet.

CHAPTER IV

MECHANICS OF WEAR

When two bodies come into contact, stresses are induced which either cause material removal from the surfaces or cause the original surfaces to conform to one another. In most cases, the maximum stresses induced by the interaction occur at some distance beneath the surfaces (15:p429,16:p257). Material removal, when it takes place, is generally from the cohesively weaker of the two bodies. The theory of wear regognizes eight different wear mechanisms, which may act singly or in combination with each other, depending on the existing rubbing conditions (15:p445,17:p59). Wear debris generated by the contact may act as an abrasive and add a third "body" or substance to the interaction, thus further complicating the situation.

Little work has been done relating these and other wear concepts to highly porous materials such as the sintered nickel chromium used in turbine seals and studied in this work. This chapter summarizes modern theories of wear with special emphasis on those applying to the rubbing interaction between turbine blades and seals.

Rubbing vs. Cutting

When moving turbine blades contact seal material (assuming that the titanium blades are harder than the porous seal material), the blades will either cut the seal material or rub the material causing a combination of elastic and plastic deformation and wear. It is essential to ascertain what causes the transition from cutting to rubbing.

According to Albrecht (14), cutting is not likely to occur unless the radius of curvature of the blade tip leading edge is small compared to the feed per pass. Consider a situation in which the tool is fed toward the workpiece by some constant increment prior to each pass. If the blade tip leading edge radius is larger than the feed on the first pass, the blade is not likely to cut the material on that pass. The material will instead deform elastically and plastically. After the blade passes (i.e. the normal force is removed) the material will spring back to its original position, minus the plastic deformation. On the next pass, the effective feed will be the sum of the feed increment plus the elastic deflection from the previous pass. If this amount is greater than the blade tip radius of curvature, cutting will occur. If not, the process is repeated. In the case of a very compliant material being rubbed by a blade with a relatively large leading edge radius of curvature, cutting may never occur.

Tool tip leading edge sharpness after grinding, as determined by an optical comparator, ranged from approximately 0.005 to 0.03 mm (about 0.2 to 1.2 mils). Since the seal material used in this experiment is extremely compliant (as evidenced by its tendency to smear), it can reasonably be expected that rubbing will occur at feeds less than the blade tip leading edge radius, and a combination of cutting and rubbing at feeds greater than the blade tip radius.

Theories of Wear

In any wear situation, material is removed from the surfaces by a combination of wear mechanisms. There are eight generally accepted wear mechanisms described in modern literature. These are adhesion, abrasion, fatigue, delamination, corrosion, cavitation, erosion, and fretting (15:p429,17:p59). Different mechanisms or combinations of mechanisms result from different rubbing conditions.

Of the eight mechanisms listed above, the final five are of lesser significance in the study of the rubbing interaction between turbine blades and seals. Corrosion wear results from chemical interaction between a component and its environment and is an important consideration in selecting materials, but does not directly relate to this study. Erosion, caused by high speed particles impinging on a surface, is a consideration in selecting seal

materials, but again, does not directly relate to the interaction between blade and seal. Similarly, cavitation (resulting from a stream of liquid containing entrapped gas bubbles) and fretting (wear due to extremely low amplitude oscillations) are not applicable. Delamination, proposed by Suh (17:p60), is only applicable to very low speed sliding in which the bulk temperature of the interface does not rise appreciably. The remaining three wear mechanisms - adhesion, abrasion, and fatigue - are more directly related to this study and will discussed in detail.

Adhesive Wear

All surfaces are rough on an atomic scale, and when brought into contact, they touch only at the tips of their asperities (Fig. 4.1). This implies that the true area of contact (A_t) is considerably smaller than the apparent area of contact. Along the areas of true contact, if the surfaces are clean, the atoms on one surface will attract those on the other, producing strong adhesion (or cold welding). As the contact load is increased, the areas of true contact grow radially and new contact locations are initiated. In other words, increasing the normal load increases the true area of contact. At infinitesimally small loads, the asperities may deform elastically. However, as the load is increased by some finite value,

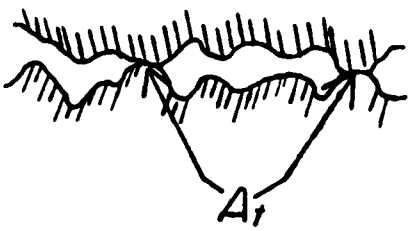

Fig. 4.1-Illustration of true area of contact at microscopic level.

local plastic deformation also occurs. For plastic contact (17:p38):

$$A_t = W/3P^*$$

where A_t is the true area of contact, W is the normal load, and P* is the yield stress of the softer material.

Upon the initiation of sliding, the adhesions formed along the true area of contact have to be sheared. The force required to shear these adhesions is the cause of the adhesive component of friction. As the adhesions are sheared, they often fracture below the surface of the weaker material, causing removal of material. For hemispheric asperities:

$$\text{Wear Volume} = BW/9P^*$$

where B is the probability that certain contacts will wear from a given number of adhesive junctions per unit sliding

distance. Thus, wear volume is a function of the normal load and yield stress of the material, but is independent of apparent contact area.

Adhesion is greatly reduced in the presence of surface contamination or lubrication and, in practice, measurable adhesion is only found when the surfaces are loaded and translated with respect to one another causing the surface films to break up (18:pF6). Adhesion is more prevalent under vacuum conditions, where surface oxides are less likely to be present.

The adhesive theory of wear has been criticized because it assumes that the materials are homogeneous and isotropic. In practice it has been found that the wear track and the layer supporting it are different in character than the original material (17:p59). This can cause the wear track to behave differently than the original material. For example, if the wear track had a differnt hardness than the original material, the rate of wear would be different than that predicted by the adhesive wear theory.

Abrasive Wear

The abrasive mechanism of wear results from hard particles or protrusions plowing through a softer surface. The softer surface, if ductile, will deform plastically. If the surface is brittle, it will be broken away. In the

ductile case, when the first pass produces a groove, repeated passes may result in removal of the material (18:pF6). During abrasion, a metal may undergo extensive work hardening and thus increase its wear resistance. When the hardness of the metal approaches that of the opposing surface, blunting or wear of the latter will occur.

According to Sarkar (17:p67), the wear rate of a metal rubbed by cone shaped asperities can be given by:

$$\text{Wear Rate} = W(.63 \cot \Theta)/H$$

where W is the applied load, H is the hardness of the metal being abraded, and Θ is the semi-apex angle of the asperities on the surface. According to this analysis, wear rate is related to load, hardness and frontal contact area, but not to apparent contact area.

Spurr (19) investigated the wear of nine different metals rubbed against abrasive papers. He found that the mechanism of abrasive wear is remarkably general and follows the form:

$$\text{Wear} = W\ K\ Up\ d/H$$

where K is a numerical constant determined by the material properties of the metals being rubbed, Up is the ploughing coefficient of friction (determined by the shape of the

abrasive particles), and d is the sliding distance. Spurr also noted that brittle materials wear more rapidly under abrasion than ductile materials.

Fatigue Wear

Fatigue wear results from cyclical loading and unloading of a surface. Fatigue is generally the result of an elastic encounter and is usually found in elastomers, but also occurs in metals. The fatigue mechanism becomes significant when adhesion is relatively small (20:p194). The number of cycles to failure, as in any fatigue situation, is related to the amplitude of the reciprocating stress and is drastically reduced by the presence of notches or stress raisers in the material.

According to Van Vlack (21:p331), fatigue wear develops in the following pattern:

1. Repeated cyclical stresses cause incremental slip and cold working;
2. A gradual reduction in ductility results in the formation of submicroscopic cracks;
3. The notch effect of the submicroscopic cracks concentrates stresses until complete fracture occurs.

Buckley (15:p504) states that the generation of cracks as a result of the fatigue process is more likely for non-homogeneous materials (e.g. two phase materials)

than for homogeneous materials because the second phase particles can act as sites for the initiation of dislocations and the growth of cavities. He further observes that fatigue cracks may initiate either in the surface or subsurface region. The subsurface crack generally progresses to the surface, possibly liberating wear particles. Surface cracks can move downward into the material and connect with other cracks, eventually resulting in wear particles. Thus, both surface and subsurface cracks which develop as a result of fatigue can lead to material removal and wear debris.

Two Body vs. Three Body Wear

Generally, rubbing interactions begin as "two body" systems - i.e. one body interacting with another. Once wear particles are generated, however, the interaction develops into a three body situation - two bodies interacting with each other as well as with the wear debris. The wear particles quite often come from the work hardened surface of a material, and are therefore harder than the substrate and new surface. As a result, wear particles trapped between the two interacting surfaces can increase forces and accelerate wear.

Location of Maximum Stresses

When two solid surfaces are brought into contact,

stresses develop in each of the materials. There is a region in the materials where the stresses are maximized. The stress distribution in the surface layer of an elastic material in contact with a rigid indentor of infinite length was described by Saverin (16:p256) and is shown in Fig. 4.2. In this case the coefficient of friction (f) was 0.4 and Poisson's Ratio for the material was 0.3. σ_1, σ_2, and σ_3 are the stresses in the X, Y, and Z directions. The ratios of σ_1, σ_2, and σ_3 to P (the maximum pressure at the center of the contact point) are plotted vs. position along the X axis of the indentor (non-dimensionalized).

In general, Saverin described the loading cycle as omnidirectional compression during the first half with σ_2 max = $-P(f+1+f^2)$ and biaxial tension during the second half with σ_1 max = $2fP$. With materials (such as ours) in which the tensile strength is significantly less than the compressive strength, the second half of the cycle is the most critical.

It is also important to note that the maximum shear stress lies some distance beneath the surface, as shown in Fig. 4.3. The stress distribution shown here is for an isotropic material, but it can be reasonably assumed that the situation is similar for non-isotropic materials. In general, the higher the friction force between the bodies, the closer to the surface the zone of maximum shear stress is. According to Buckley (15:p500), this zone of maximum

is. According to Buckley (15:p500), this zone of maximum shear stress is likely to produce subsurface cracks when cyclical loads are applied to the material surface.

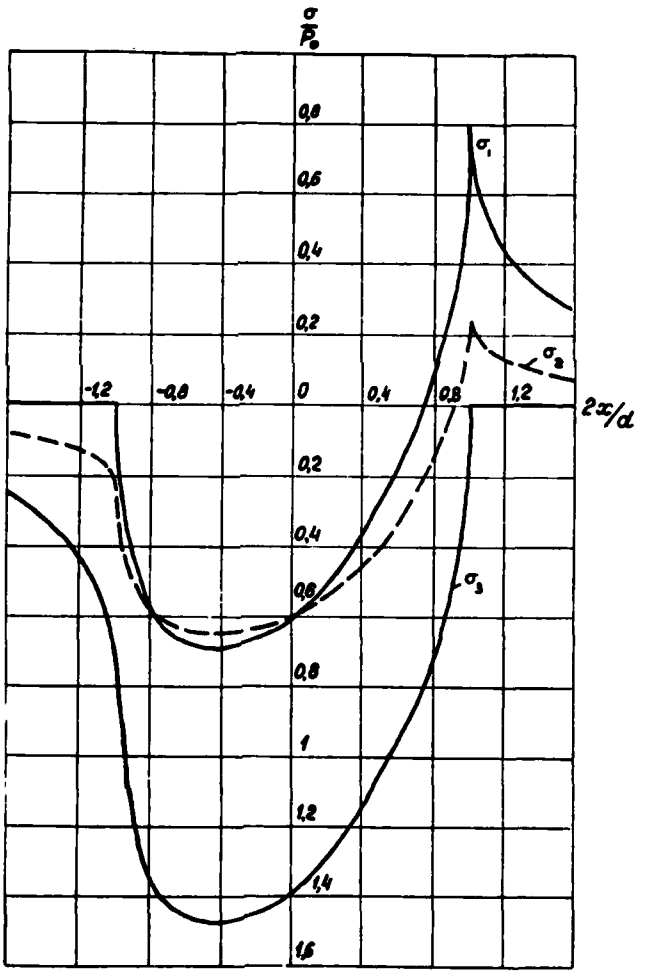

Fig. 4.2 - Stress distribution in the surface layer of a stationary elastic material in contact with a rigid body. The rigid body is moving from right to left (16).

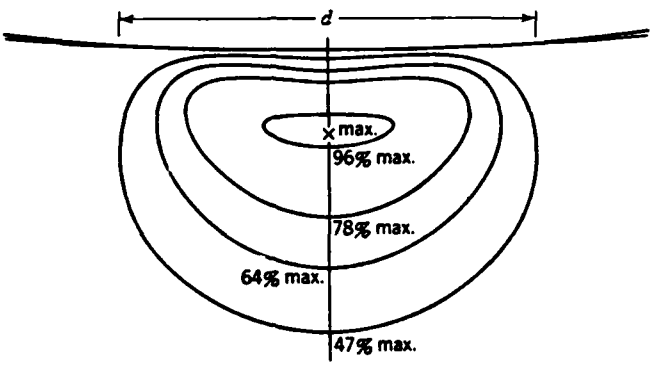

Fig. 4.3 - Section view of the shear stress distribution beneath a surface over which a rigid body slides. The rigid body is sliding toward the reader (15:p430)

CHAPTER V

RESULTS AND DISCUSSION

Several significant findings were made during the tensile and low speed rub tests. The presentation of these findings within this chapter is divided into 12 sections. Each section contains a discussion of the results as they are presented.

Tensile Tests

Two tensile tests were performed on the seal material, and the stress-strain relationships obtained during these tests are shown in Figs. 5.1a and b. The ultimate tensile strength in both cases was about 75% of the manufacturers value (7.3 MN/m^2). The dashed lines on Figs. 5.1a and b represent points during the tests where the load was relaxed and then reapplied. Especially interesting is the fact that the modulus of elasticity (E) for this material varies considerably with strain. E increases as the material is compressed and decreases as the material is stretched.

Results from the tensile tests were combined with compression test results reported by Wolak et al (9) and are shown in Fig. 5.2. During the tensile tests, E initially decreased rapidly with strain but then tended to

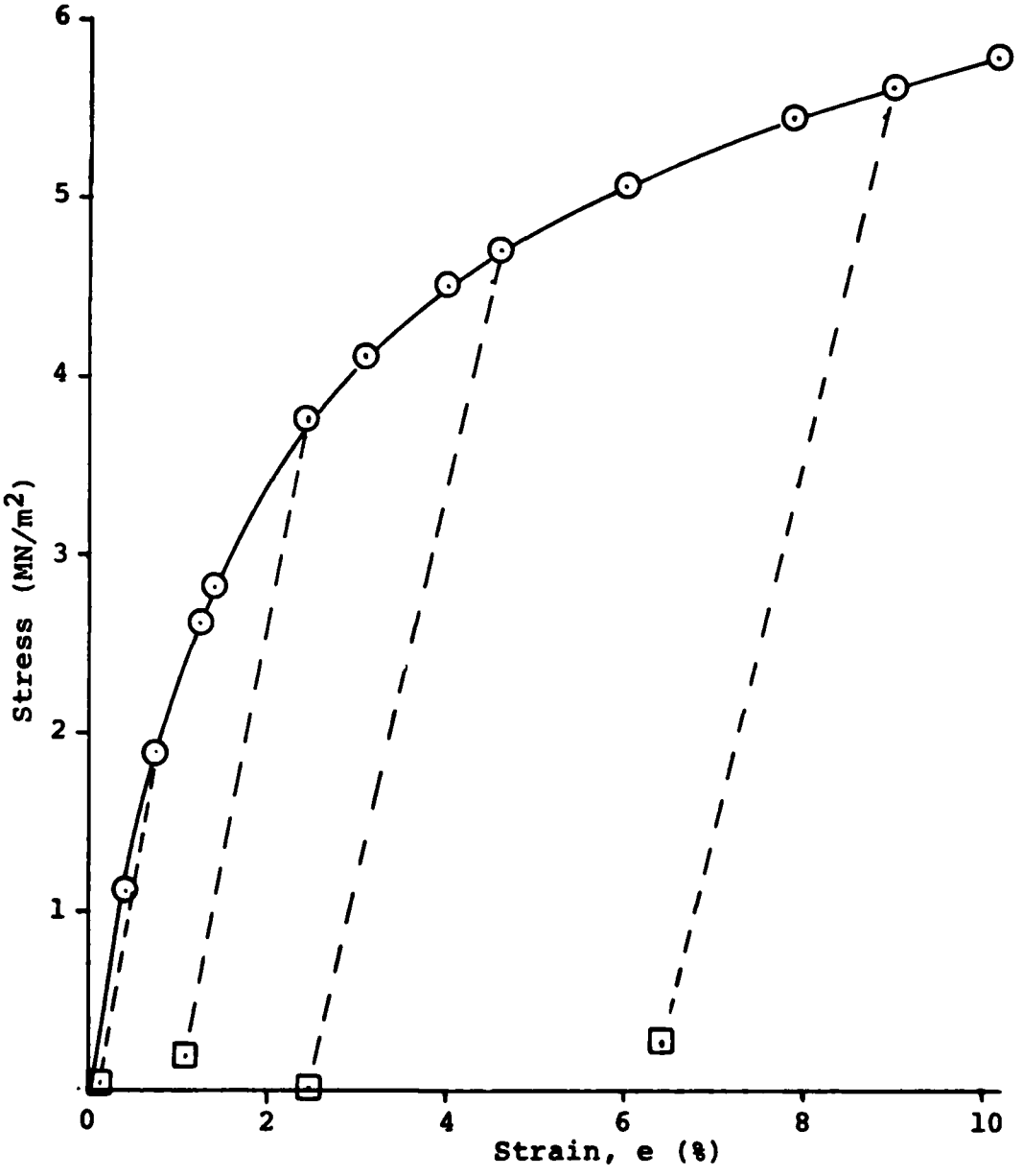

Fig. 5.1a- Stress-strain curve from tensile test #1.

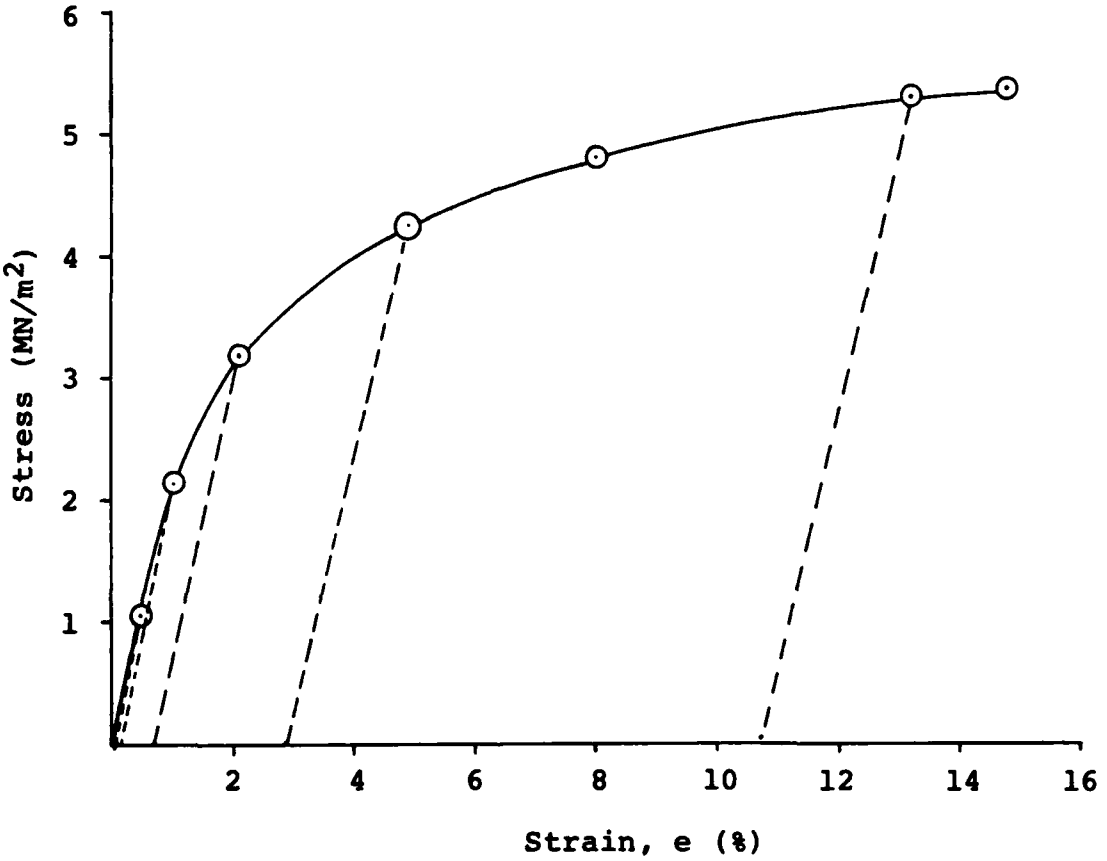

Fig. 5.1b- Stress-strain curve from tensile test #2.

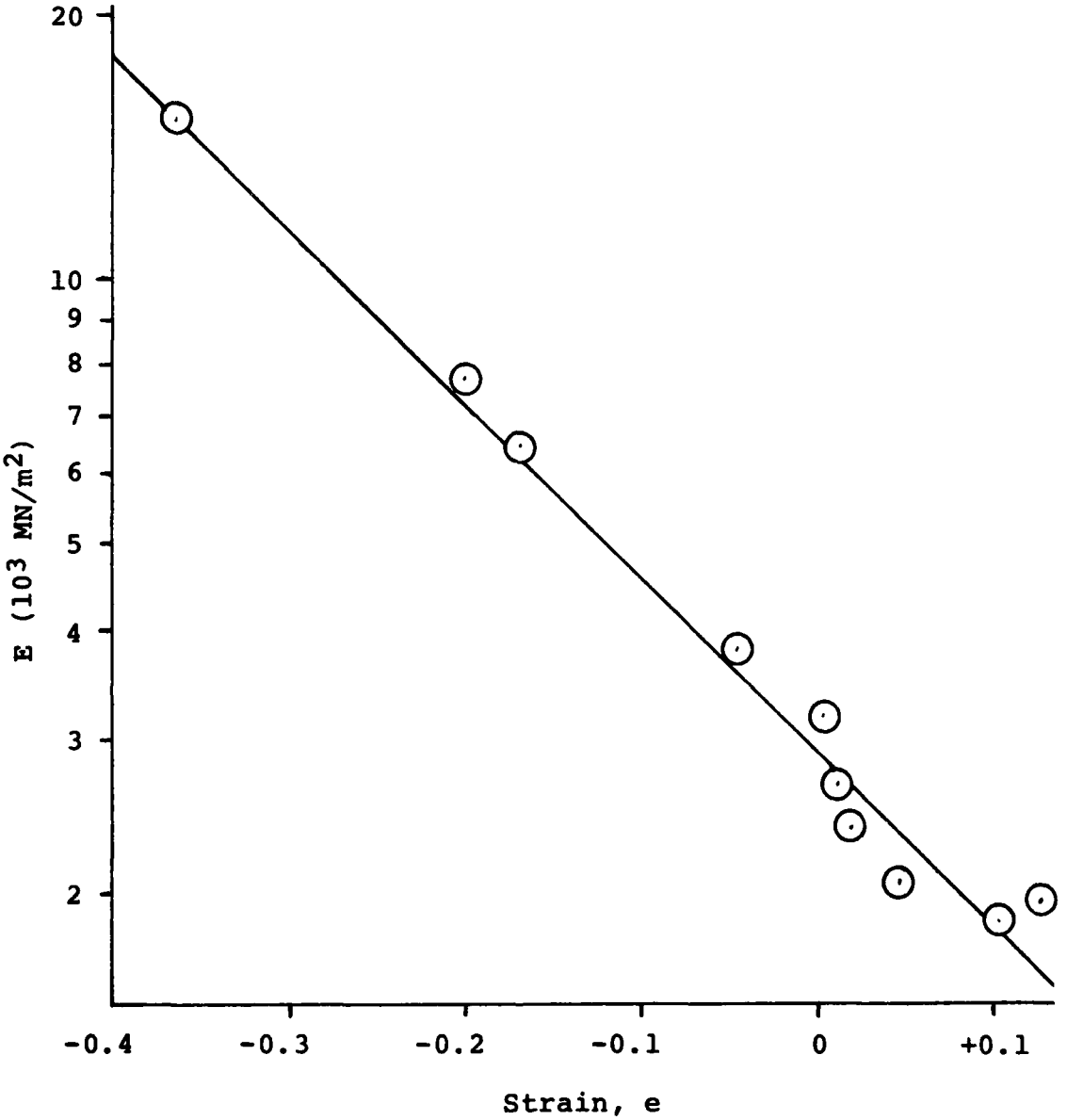

Fig. 5.2 - Modulus of elasticity vs. strain from compression (9) and tensile tests of seal material.

level off. One explanation for this is based on the structure of the seal material (porous, sintered particles). When the tensile load is first applied, some of the weaker interparticulate bonds are easily broken, thus decreasing E. As the load increases, the particles tend to align themselves along the direction of the load axis, and E stabilizes until final fracture occurs. In compression, the weaker bonds are not broken. Instead, E increased with density as the material was compressed, and probably reached a maximum value somewhat less than E for a 100% dense specimen made from the same alloy.

The curve in Fig. 5.2 can be expresed by:

$$E = E_o \times 10^{C2\ e} \qquad \text{(Eqn 5.1)}$$

where E_o = 2.95 MN/m (the approximate value of E at zero strain), C2 = -1.96 (derived numerically) and e is the strain at the point in question.

The fact that E increases with compression has an important implication for the rub tests: it can be expected that a given amount of deflection will require a greater force as the material densifies and E increases.

Rub Test Forces

Throughout the rub tests, the forces varied in magnitude during each individual rub as shown in Fig. 5.3.

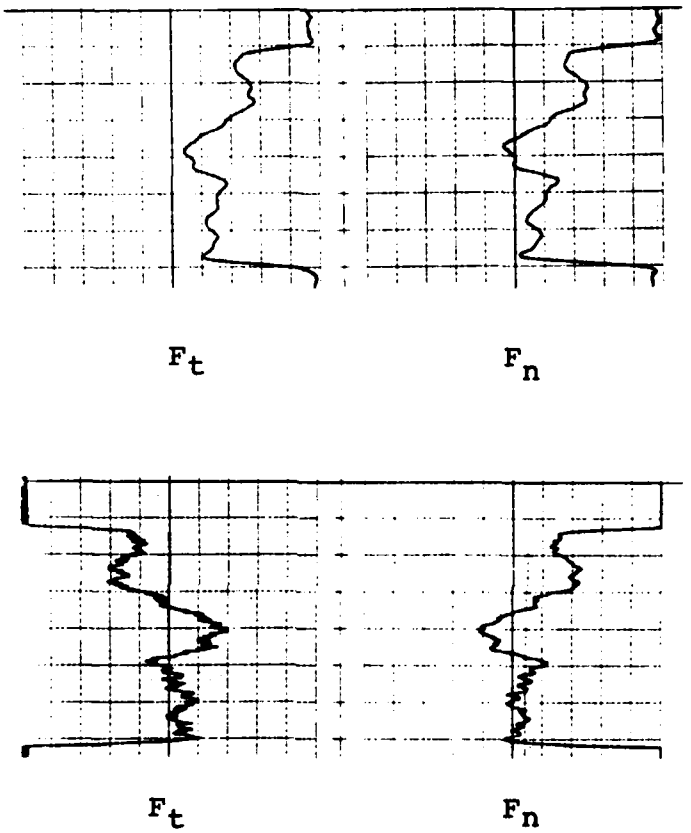

Fig 5.3 - Records of typical rub forces sensed by the strain gage dynamometer (top) and the piezo-electric dynamometer (bottom) from test #26. The bottom of each record corresponds to the start of the rub. The apparent difference in magnitude between the two dynamometers is due to different sensitivity/amplification settings. In actuality, agreement between the two dynamometers was within 5%.

There are several reasons for this variation. First, since the seal material is made up of sintered particles, it is not homogeneous, so some force variation could be expected along the length of the rub path. Also, it is possible that some seal material particles could be removed by the blade at one end of the seal and pressed into the seal at the other end. Although the loose particles were carefully vacuumed or blown away between rubs, a small number may have been transported by the blade, producing a density gradient along the rub path. Finally, when smearing occurred, it tended to start with small isolated patches of smeared material which eventually either grew together or were removed after a number of rubs as new patches were forming. As a result, forces varied as the blade passed between smeared and unsmeared areas on the seal.

In order to make the data more meaningful, average forces were considered in analyzing the rub interaction. Average forces were obtained using the equation:

$$F = \int_0^L F(L)\, dL/L$$

where F(L) is the location varying normal or transverse force along the length of contact L. The average force value was obtained with a planimeter or, when possible, by inspection.

Effect of Densification on Forces

In general, rub forces increased with incursion. As

seen from the stress-strain curves derived from the tensile and compression tests, the rate of force increase depends to a large degree on the amount of densification produced in the seal.

Fig. 5.4 shows the surface of the seal specimen used during test #28, along with the forces recorded at approximately the same time as the photo was taken. This photo demonstrates the fact that forces vary with the amount of smearing present at the rub interface.

In those cases where material was worn or cut away faster than it was plastically deformed, forces increased less quickly, leveled off, or in some cases actually decreased. Examples of this behavior were seen during those portions of tests #26 through 28 which utilized feeds of 0.625×10^{-6}m/pass or less. For further discussion, see "Effects of Varying Feed Within a Test", this chapter.

Effect of Blade Tip Radius

As previously mentioned in Chapter IV, the radius of the leading edge of the square ended blades used in these tests was approximately 0.005 to 0.03 mm. Tests #19 and 20 had feeds of 0.05 and 0.10 mm respectively, and, as expected, material was removed by cutting. The normal forces encountered in these tests are shown in Fig. 5.5 along with the results from test #11, which had a feed of

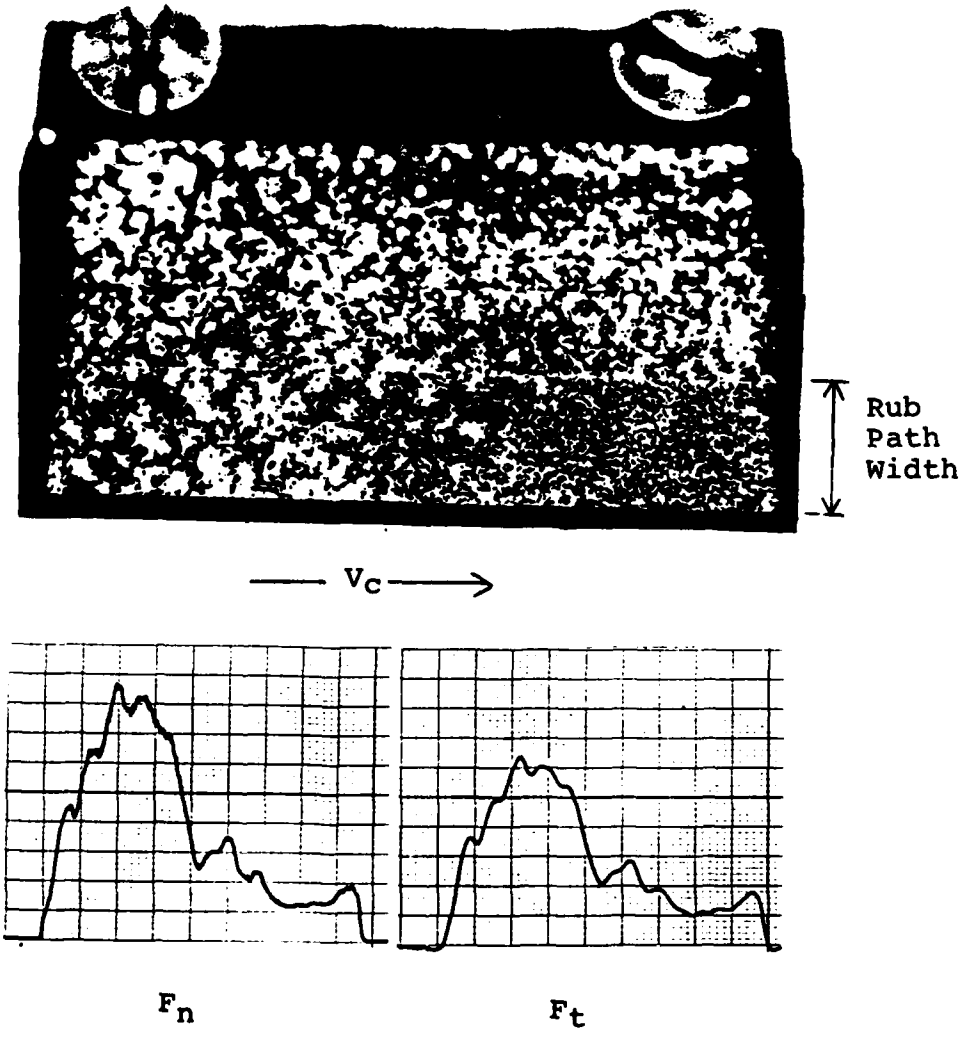

Fig 5.4 - Variation of forces with amount of smearing on seal surface. Bright areas on seal (top) are smeared.

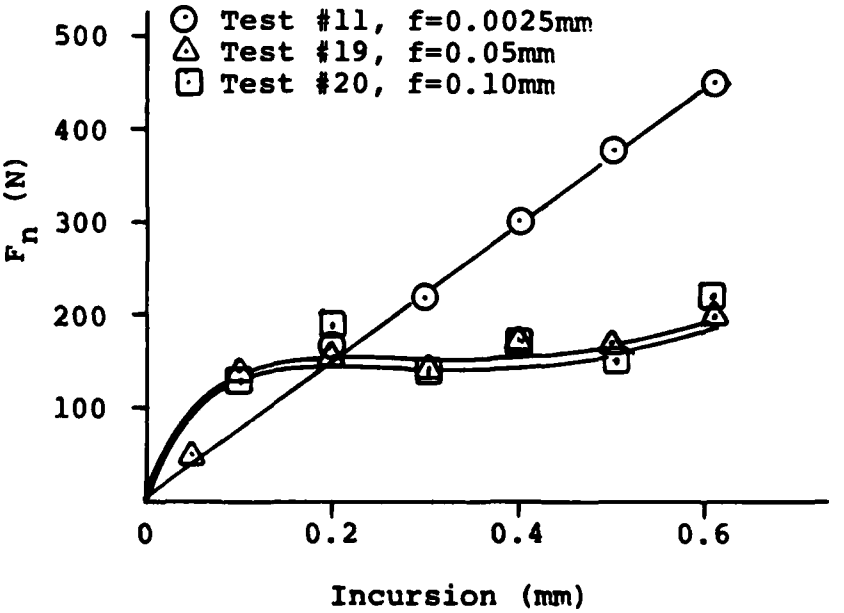

Fig. 5.5 - Effect of blade tip radius (square ended blade). Test #11, with small feed compared to blade tip radius, shows steadily increasing forces as the seal material densifies. Tests #19 and 20, with large feed compared to blade tip radius, shows forces leveling off because of cutting away of the seal material.

0.0025 mm. In tests #19 and 20, the normal forces rose quickly and then leveled off at relatively constant values. The seal densification factors for these tests were extremely low (0.07 and 0.15 - see Table 5.1), indicating that the seal material was being abraded rather than densified, although a small amount of densification occured. Test #11, on the other hand, had continuously increasing forces and a high densification, Sd = 0.70.

Test #7 is also of considerable interest at this point. The feed used in Test #7 was 0.0125 mm/pass, approximately equal to the blade edge radius. A plot of Fn vs incursion (Fig. 5.6) shows a transition point where the normal forces suddenly begin to increase rapidly after a period of lower forces. It was observed that particles were removed during the first portion of the test, but the material began to densify at about the time the forces began their rapid increase. The probable cause of this transition is that the leading edge of the blade wore during the test, resulting in a larger leading edge radius and a subsequent transition from cutting to rubbing. The seal densification for this test had a moderate value of 0.47.

Blade Tip Lay

Rubbing conditions for Tests #22 and 23 were identical in all respects except for blade tip lay. The

Test #	Rake Angle	Feed (10^{-6}m)	Vc (cm/s)	*Blade Lay	Sd
7	90	12.5	1	2	0.47
8	90	12.5	5	2	0.95
9	90	12.5	10	2	0.82
10	85	12.5	5	1	0.99
11	90	2.5	5	2	0.70
19	90	50.0	1	2	0.07
20	90	100.0	1	2	0.15
21	85	50.0	1	2	0.97
22	85	100.0	1	1	0.88
23	85	100.0	1	2	0.73
26	85	Variable	5	2	0.28
27	85	Variable	5	2	0.35
28	85	Variable	5	2	0.29

*Blade lay: 1 = parallel to Vc, 2 = perpendicular to Vc.

Table 5.1 - Seal densification factors (Sd) for low speed rub tests.

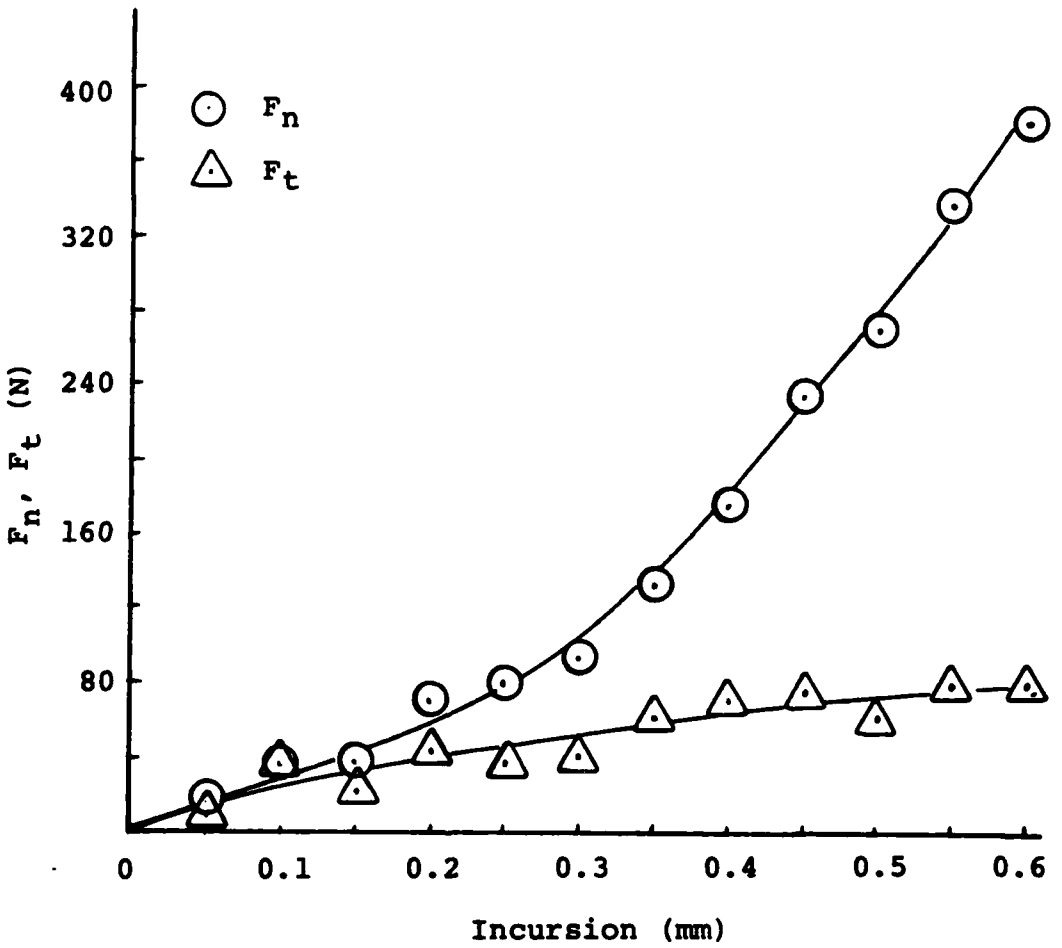

Fig. 5.6 - Rub forces during test #7. Slope of F_n plot begins to increase at approximately 0.3 mm, concurrent with transition from cutting to rubbing.

blade used in test #22 was ground parallel to the rubbing direction, while the blade used in test #23 was ground perpendicular to the rubbing direction. Forces encountered during the tests are shown in Fig. 5.7. Although Fn was essentially equal for the two tests, Ft was somewhat higher for test #23. This was probably due to greater mechanical interference between the irregular surface of the seal and the ridges on the blade tip, which were produced during grinding. In addition, Sd for the parallel blade tip lay (0.88) was higher than for the perpendicular lay (0.73), suggesting less wear in the parallel case.

Rubbing Speed

Rubbing conditions for tests #7, 8 and 9 were identical except for cutting speed. Fig. 5.8 is a plot of Fn vs incursion for these three tests. Fn was essentially equal in tests #8 and 9, indicating that the change in Vc from 5 to 10 cm/sec had little effect on forces. Fn in test #7, however, was considerably lower than in the other two tests. Upon closer examination of the results, the following explanation may be offered. Sd was significantly lower in test #7 (0.47) than in test #8 (0.95) and #9 (0.82) because more cutting occured in test #7 than in the other two tests. As a result, forces were lower in test #7. The probable reasons that more cutting occured in test #7 are:

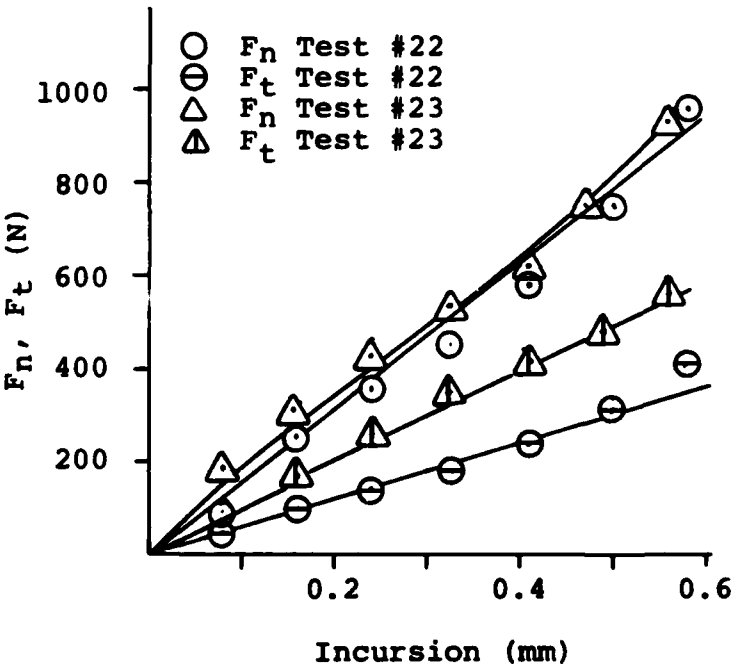

Fig. 5.7 - Rub forces vs. Incursion for blades having blade tip lay parallel (test #22) and perpendicular (test #23) to rubbing.

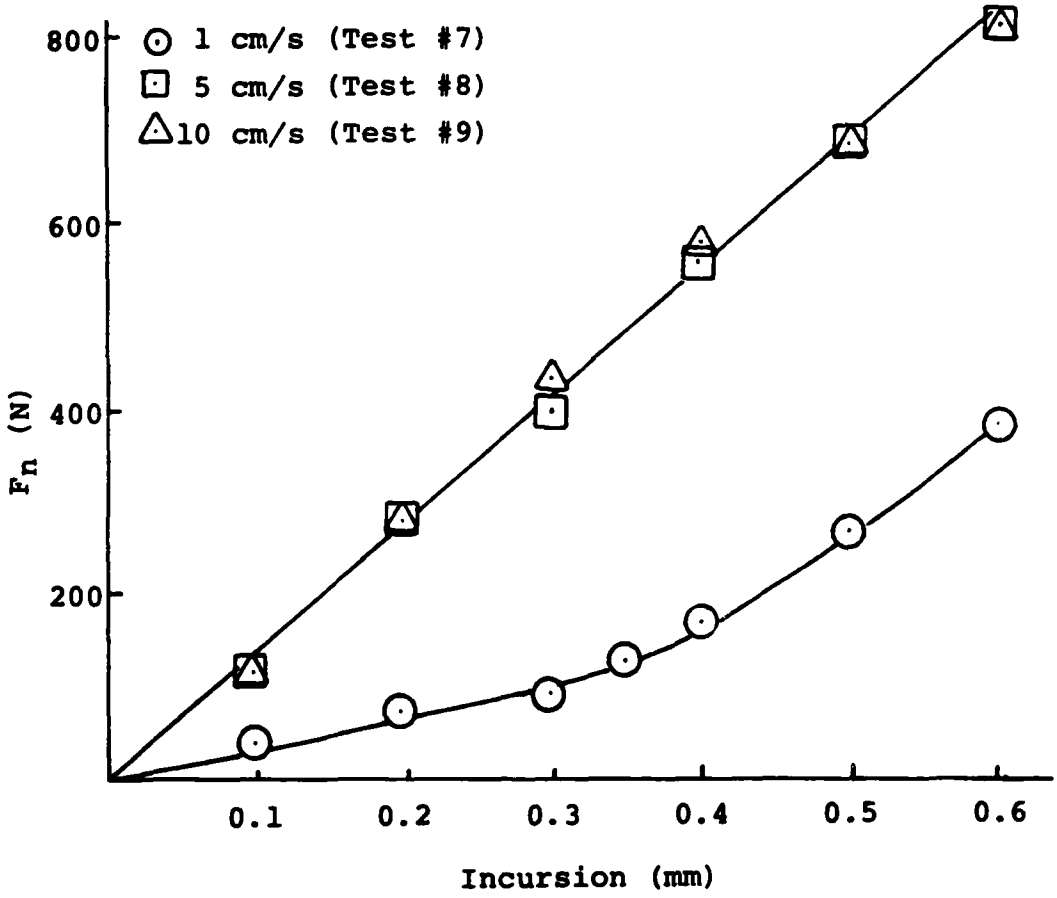

Fig. 5.8 - Effect of cutting speed (V_c) on normal force (F_n). Test #7 had cutting during first 0.3 mm of test, resulting in lower forces.

1. the blade tip leading edge radius was slightly smaller in test #7 than in the other tests;
2. the blade tip wear was slightly faster at the faster cutting speeds in tests #8 and 9;
3. a combination of the above.

Fig. 5.8 suggests that after approximately 0.3 to 0.4 mm total incursion, when smearing began to increase and cutting decreased, the slope of the line associated with test #7 approximated the slopes in the other tests. It can be concluded, therefore, that Vc had a relatively minor effect on Fn during rubbing for the speeds used in this work.

Comparison With High Speed Rub Tests

Low speed rub test results corresponded surprisingly well with those reported by Wolak et.al. (9,22) for high speed rub tests. Low speed test #27 is compared below in Table 5.2 with high speed test #40. Rake angle and feed for the two tests were approximately equal.

Test #	Vc (m/s)	Rake Angle	feed (10^{-6}m/pass)	*Fn	*Ft	Sd %
27	0.05	-85.0	0.156	40N	22N	35.0
40	100	-85.4	0.152	28N	17N	5.3

*Average force at 0.6mm incursion

Table 5.2 - Comparison of results from low speed test #27 and high speed test #40.

There were at least two differences (besides Vc) between the two tests and the way the results were analyzed. First, because several different feeds were used during test #27, and two of them were higher than the 0.156×10^{-6}m/pass feed being considered here, the seal densification factor shown in Table 5.2 for test #27 is probably higher than it would have been if the feed used in test #27 was a constant 0.156×10^{-6}m/pass (see "Effects of Feed Rate", this chapter). As a result, the forces from test #27 were also probably higher than they would have been with a constant feed of 0.156×10^{-6} m/pass. Second, the high speed test apparatus utilized a flat seal surface being fed against a rotating blade (Fig. 1.7). This caused the depth of incursion to vary along the arc of contact, with the greatest depth approximately at the center of the arc. The depth of incursion in the low speed tests, on the other hand, was essentially constant along the length of contact. This leads to some difficulty in comparing average forces. It is reasonable to assume that the average forces in the high speed test would have been somewhat higher if the incursion had been constant throughout the rub. An even closer agreement in the results might be obtained if these two differences were eliminated.

Effects of Feed Rate

Five different feed rates were used during this experimental work: 0.63, 2.5, 12.5, 50.0 and 100.0 X 10^{-6} m/pass. A sixth feed rate, 0.16 X 10^{-6} m/pass was simulated by feeding 0.63 X 10^{-6} m every fourth pass. On all tests except #26 through 28, feed was constant. Tests #26 and 27, which concentrated on small feeds, varied between several different feeds within each test to increase the amount of data collected. In addition, feed was stopped at several points during tests #26 through 28 to examine the rubbing interaction at "zero feed". Also, a significantly greater amount of blade wear occured during these tests than during the higher feed tests, so incursion (I) into the seal material was obtained by the following formula:

$$I = C - K$$

where C is the total infeed (number of passes times the feed), and K is the change in blade length due to wear.

Figs 5.9 and 5.10 show plots of Fn vs Incursion at varying feeds. Fig 5.9 contains data from those tests which used slanted (-85 degree rake angle) blades, and Fig. 5.10 shows results obtained using square ended blades. Only the results from tests #8 and 11 are shown in Fig. 5.10 because square ended blades used at greater feeds removed seal material by cutting, as previously discussed in "Effect of Blade Tip Radius", this chapter.

It is clear that force increased dramatically with

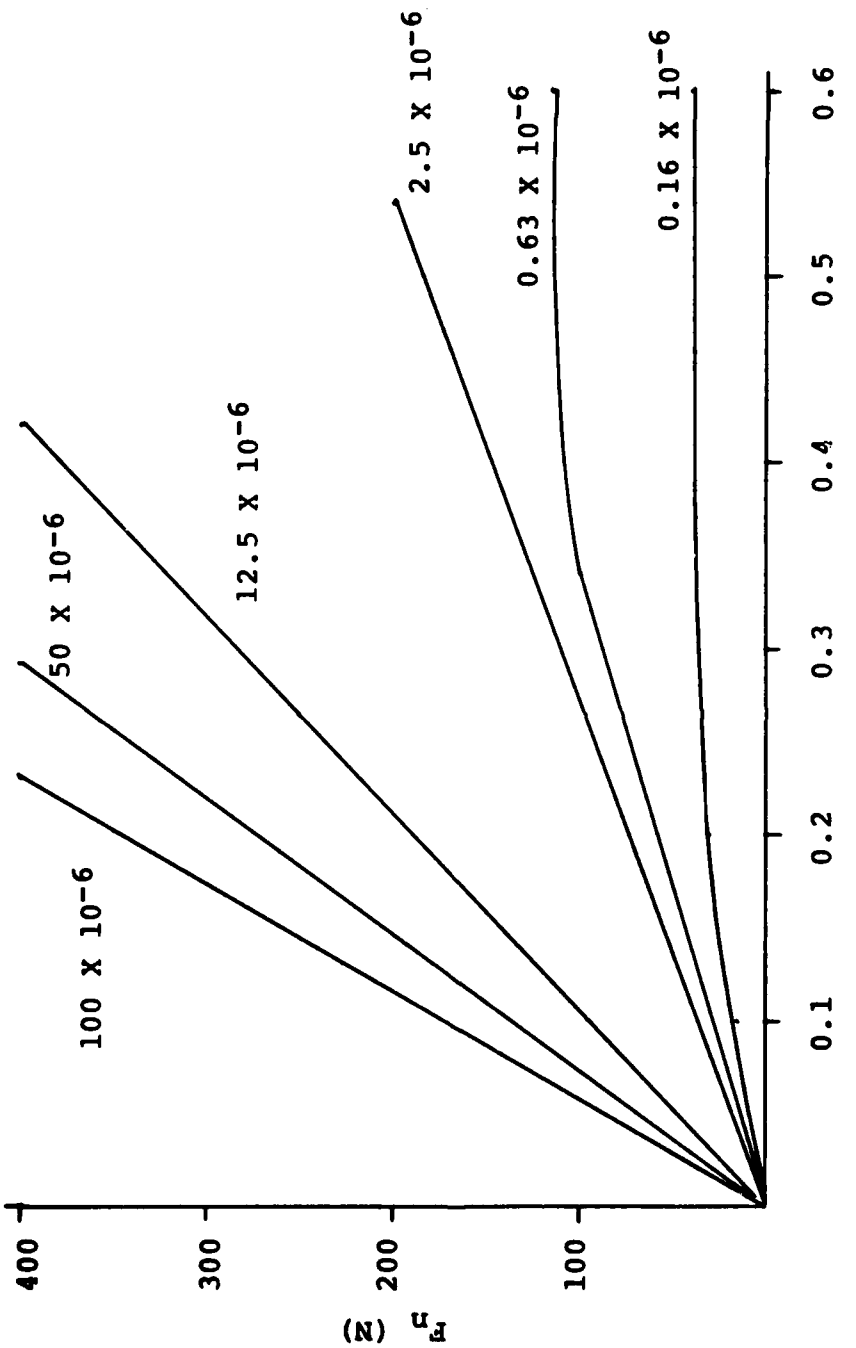

Fig. 5.9 - Effect of feed on normal force (F_n) for slanted blades. Feed is given in m/pass.

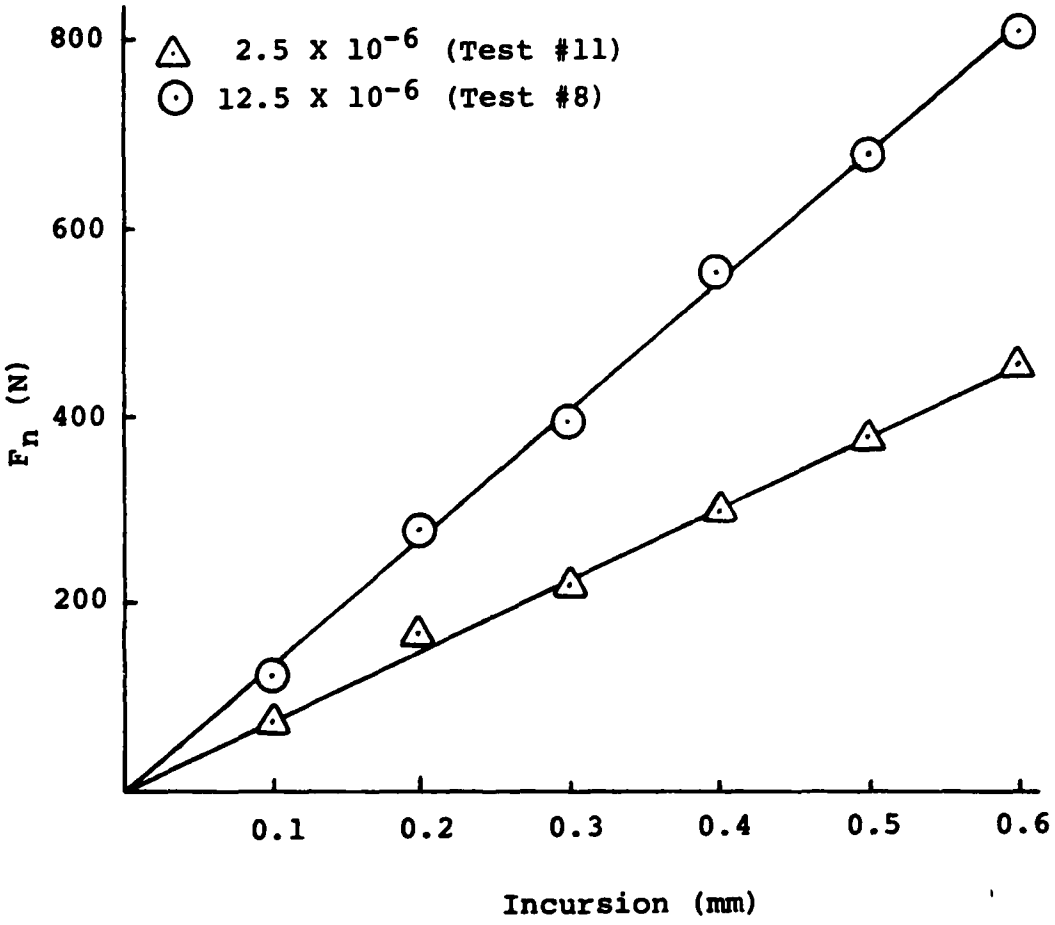

Fig. 5.10 - Effect of feed on normal force (square-ended blades). Forces are noticeably lower at the smaller feed used in test #11. Feed is given in m/pass.

increasing feed rate. There are three apparent reasons for this. First, a larger feed means that more seal material has to be displaced on each pass. Second, in those tests in which slanted blades were used blade tip area increased as the blade wore. This is likely to contribute to an increase in forces as the test progressed. Third, the results of this experiment show that seal material wear is dependent upon the number of rub interactions. In other words, at very low feeds seal wear per unit of infeed was greater than at high feeds, even though forces were much smaller than at high feeds. In fact, at the two smallest feeds, equilibrium conditions were established after a number of passes, wherein the forces remained constant or decreased with increasing incursion. This suggests that seal densification had stopped increasing and that the rate of seal wear was greater than or equal to the feed. Values from Table 5.1 for slanted blade tips show Sd to be considerably lower for tests #26 through 28, which had very low feed rates, than for tests #10, 21 and 23, which had higher feed rates. Fig. 5.11 is a crossplot of Fn at 0.3 mm incursion for various feed rates. Forces remain low for the three smallest feeds because the seal material wears at approximately the same rate as the blade is fed, and, therefore, densification is low.

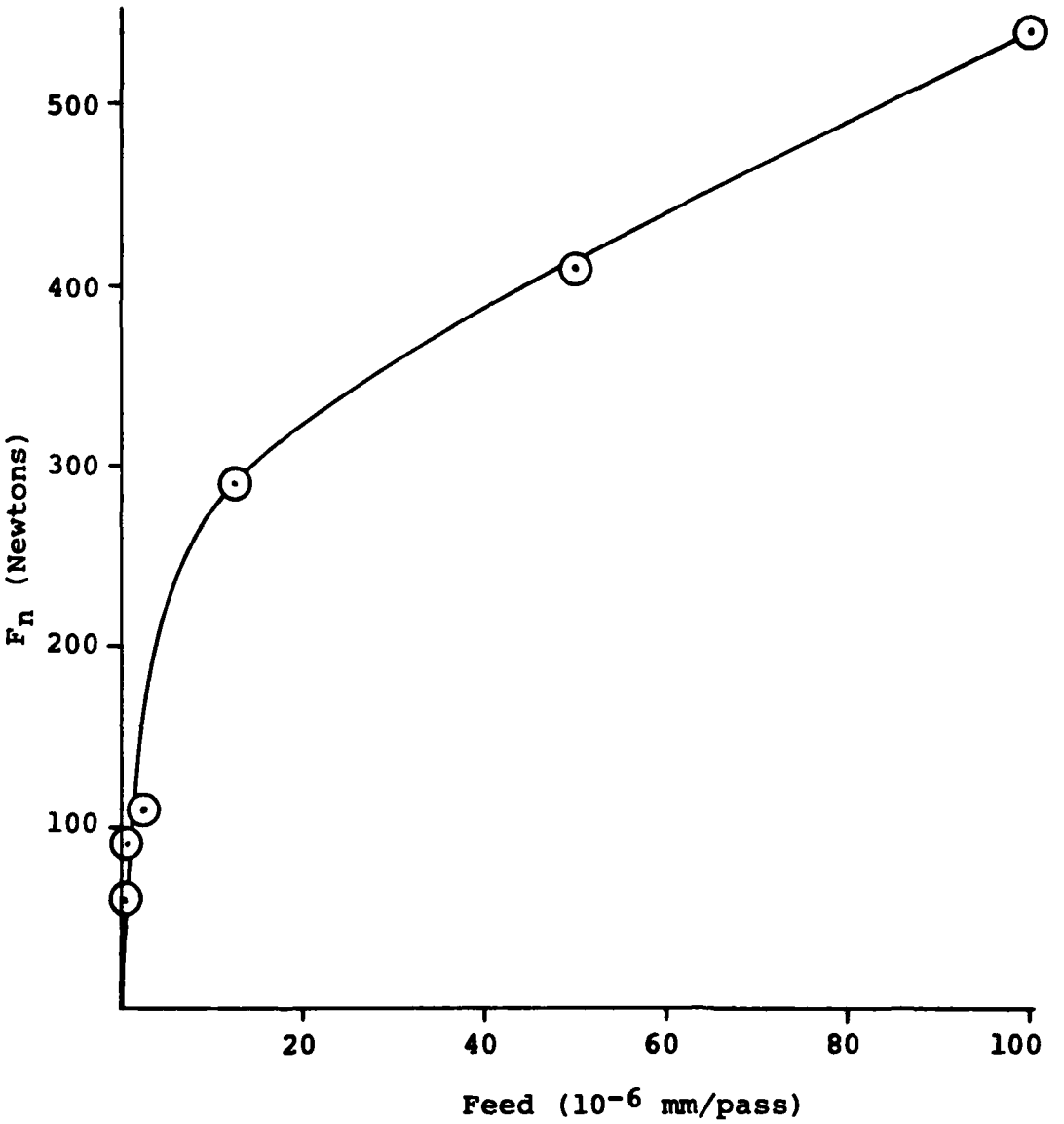

Fig. 5.11 - Normal force (F_n) vs. Feed at 0.3 mm incursion for slanted blades.

Effects of Varying Feed Within a Test

Changing the feed during a rub test had a significant effect on rub forces. Three cases - increasing, decreasing and stopping feed - were examined and are discussed below.

a. Increasing Feed

When feed was increased during a test, rubbing forces also increased, as expected. The rate of increase of the forces, however, was not constant. Fig. 5.12 is a plot of Fn vs. incursion for a portion of test #27. Four different feed rate segments are shown in Fig. 5.12: between 0.32 mm and 0.45 mm incursion, $f = 2.5 \times 10^{-6}$ m/pass; at 0.45 mm incursion, f = zero for approximately 200 passes; between 0.45 mm and 0.52 mm, $f = 0.16 \times 10^{-6}$ m/pass; between 0.52 mm and 0.57 mm, $f = 0.63 \times 10^{-6}$ m/pass; and between 0.57 mm and 0.75 mm, $f = 2.5 \times 10^{-6}$ m/pass. Each time the feed rate is increased, there is a period of rapid increase in force followed by a slower increase (or constant force as in the case of $f = 0.16 \times 10^{-6}$ m/pass). The final rate of force increase appears to approximate that of the previous segment of the test which had the same feed rate.

b. Zero Feed

Feed was stopped several times during tests #26-28, and in each case, forces decreased with each subsequent pass. This indicates that wear of the seal and/or blade continued due to the elastic forces in the system. Plots made of Fn vs. Number of Passes (N) indicate an

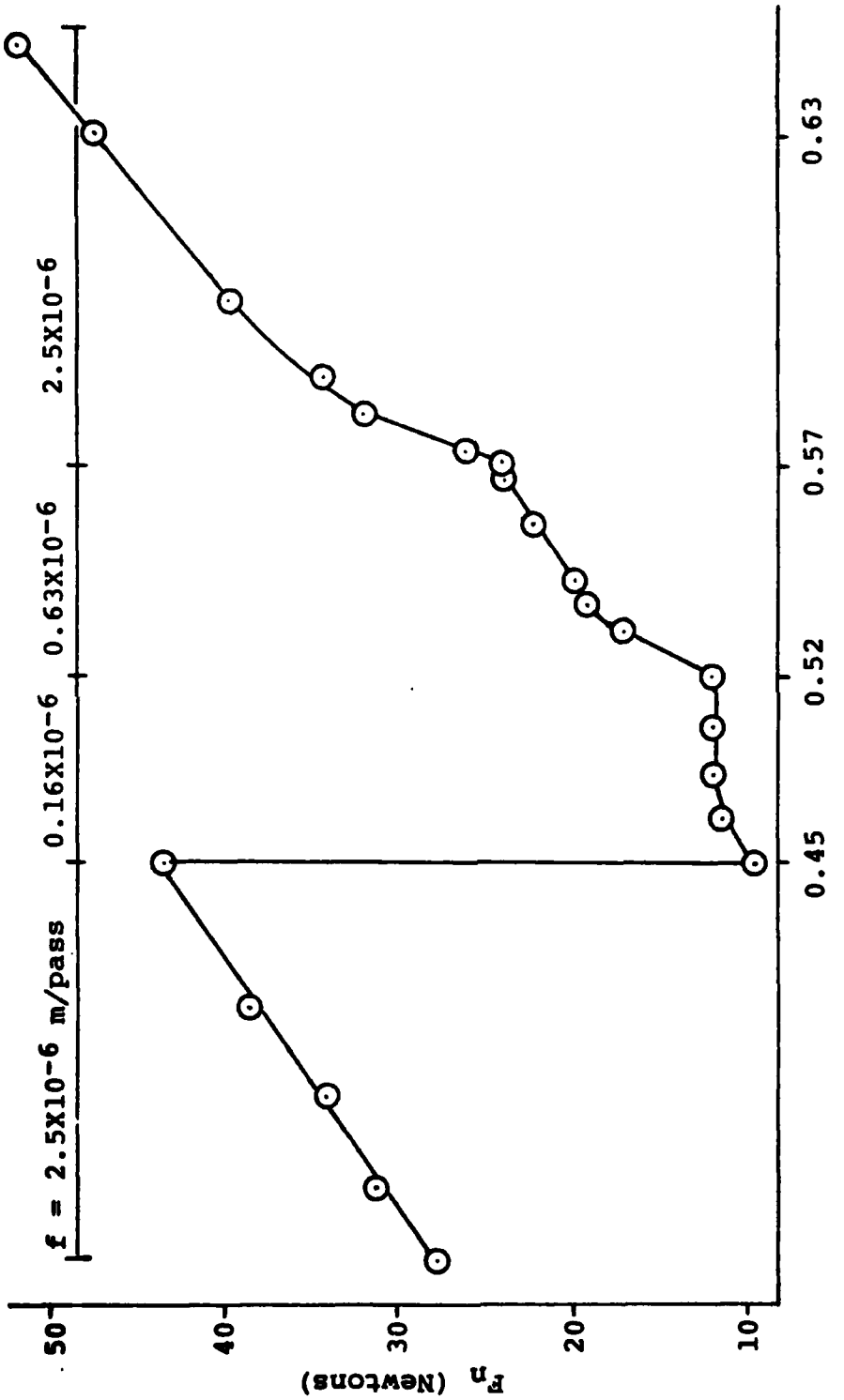

Fig. 5.12 - Effect of increasing feed during a rub test. Feed for each segment is shown at top.

exponential decay of forces as rubbing continues (Fig. 5.13). Furthermore, a linear relationship exists between Log (Log (FN)) and N, as shown in Fig. 5.14. Based on this information, the following equation was derived as a first approximation to determine Fn for the curve labeled (a):

$$Fn = Fn_o^{(10^{(-0.0027N)})} \qquad \text{(Eqn. 5.2)}$$

where Fn_o is the normal force (in Newtons) when feed is stopped and N is the number of passes at zero feed. This equation yields values within 10% of the actual values measured during testing. One exception (labeled "b" on Fig. 5.14) was encountered during test #26, in which Fn decayed more rapidly than in the other cases. This occured early in the test when blade wear (and therefore blade tip area, R) was small. This suggests that seal material is more easily removed by a small area blade tip than by blade tips with larger areas.

c. Decreasing Feed

As feed rate was decreased, forces also decreased, as expected. Results were similar to those found with zero feed: the forces followed an exponential decay until established on the linearly increasing portion of the segment. Fig. 5.15 shows a porion of test #27 during which feed rates were decreased in several segments. On Fig.

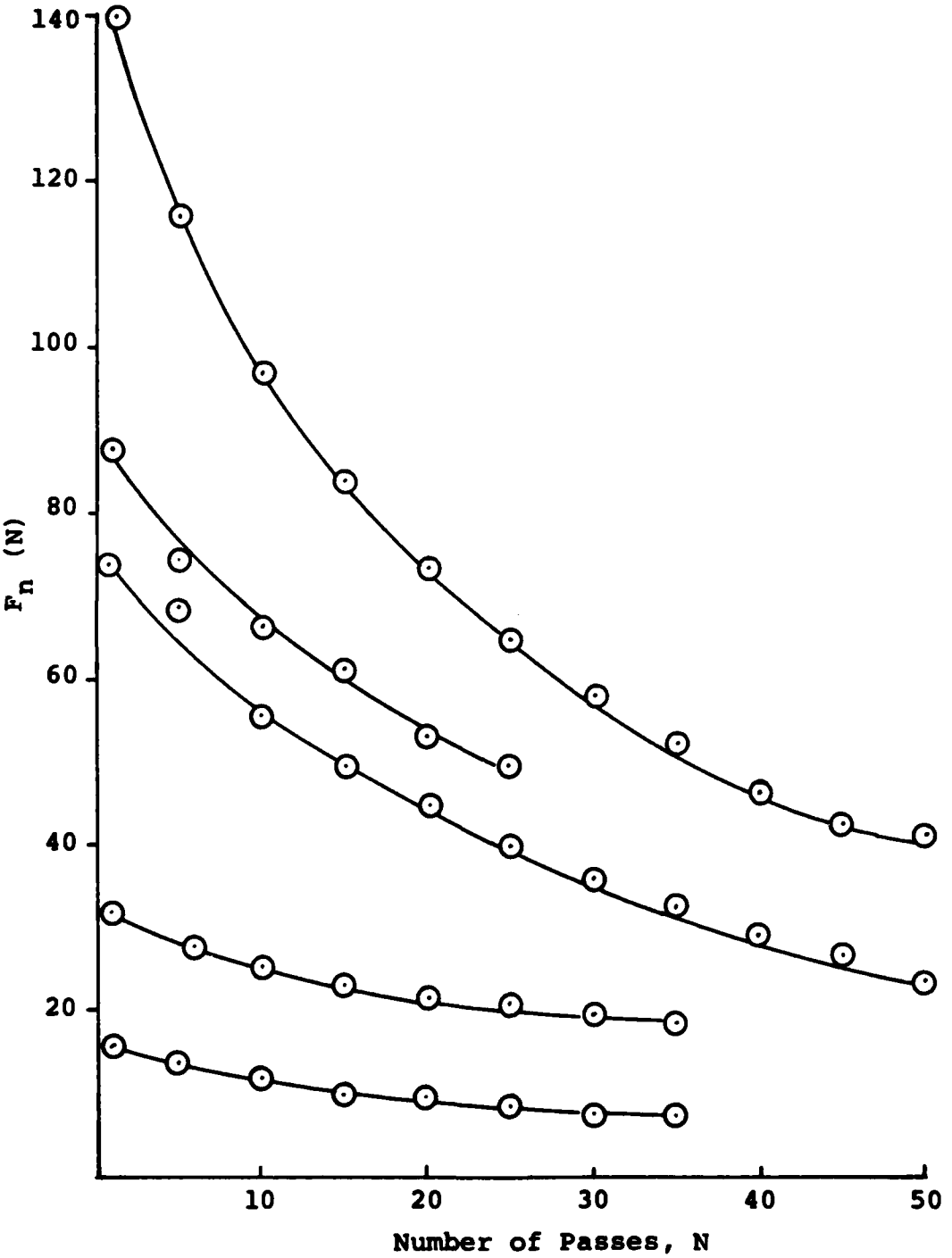

Fig. 5.13 - Decay of forces after feed is stopped.

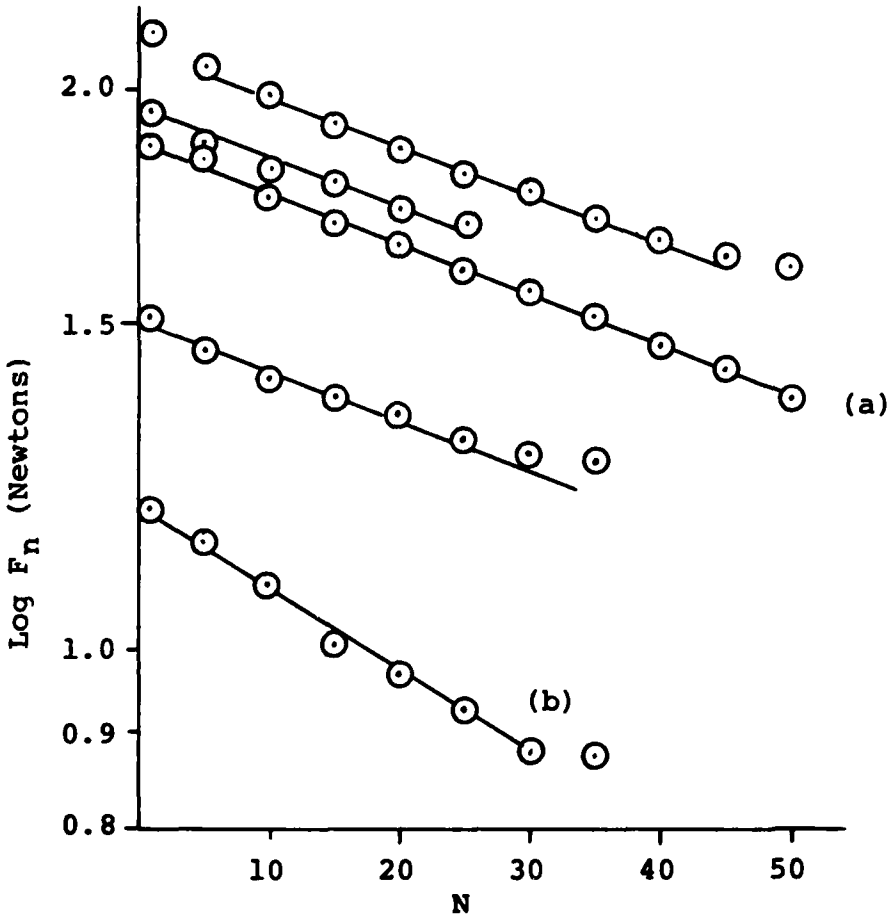

Fig. 5.14 - Log(Log(F_n)) vs. Number of Passes (N) at zero feed. Data taken from tests #26-28.

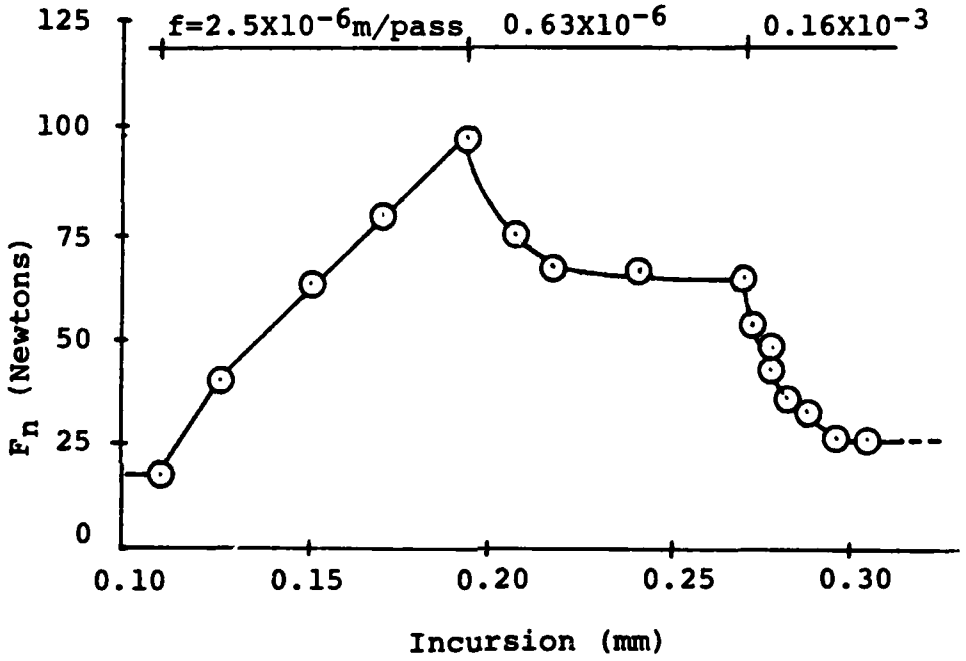

Fig. 5.15 - Effect of decreasing feed during a rub test. Data taken from test #27. Feed for each segment is shown at top.

5.15, the feed rate was the same at the end of the plot as it was at the beginning, with constant forces at both ends of the plot.

Change in Elastic Forces With Blade Tip Area

The normal forces encountered during these rub tests resulted from feeding the blade against the seal, thereby depressing the seal. It is reasonable to expect, therefore, that increasing the size of the blade tip area would increase the normal force for a given amount of deflection. Since E changes with seal densification, any discussion of elastic forces must be based upon a known amount of densification. Fig. 5.16 shows Fn vs. deflection curves for various blade tip thicknesses (R), assuming E = 2.95×10^3 MN/m^2 (i.e. zero densification). Edge effect is neglected, and the remainder of the system (dynamometers, blade and planer) were assumed to be rigid. Calculations were based on a blade width of 12.7 mm and a seal thickness of 3.0 mm.

Specific Energy of Material Displacement

The specific energy of material displacement (Ps) is defined as the energy required to displace (i.e. either remove or densify) one gram of seal material through rubbing (see Appendix B). Fig. 5.17 is a plot of ln (Ps) vs. ln (feed) at 0.5 mm incursion. From this plot it can

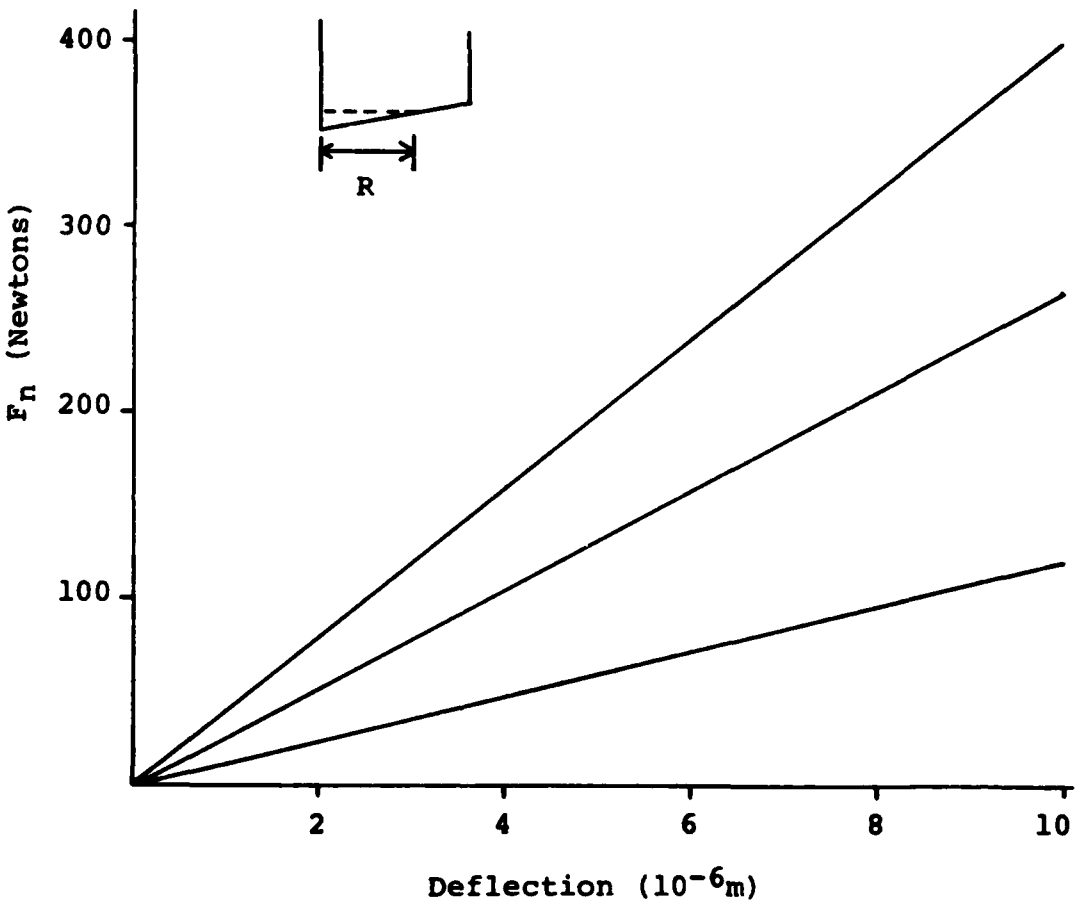

Fig. 5.16 - Plot of normal force (F_n) vs. Deflection of seal material for various blade tip thicknesses (R), assuming no edge effect, no plastic deformation, zero densification of the seal material, and a rigid system. Blade width is 12.7 mm and seal thickness is 0.3 mm.

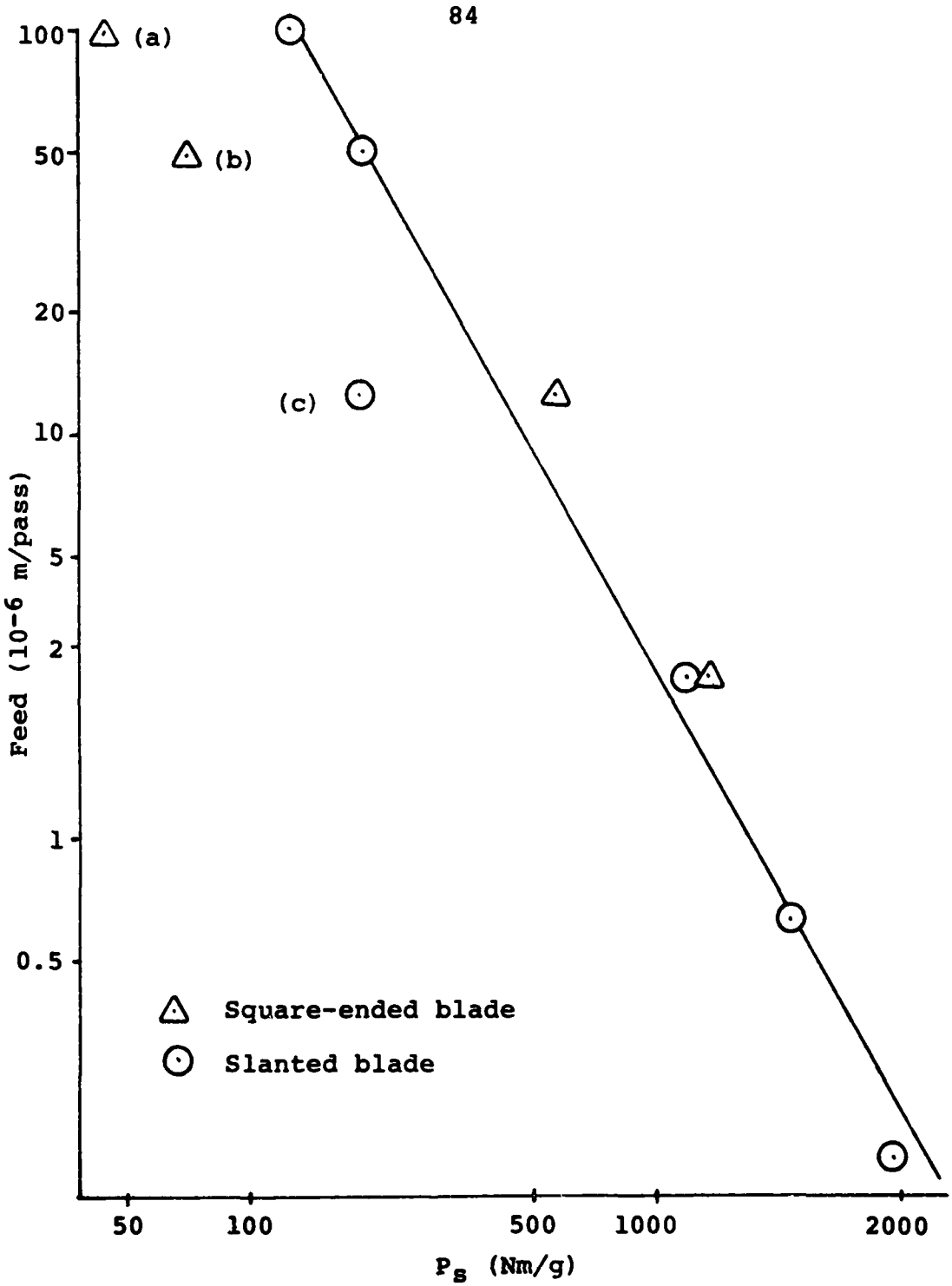

Fig. 5.17 - Feed vs. Specific Energy of Seal Displacement (P_s).

AD-A132 354 WEAR DURING RUBBING OF A SINTERED METAL POWDER BODY(U) 2/2
AIR FORCE INST OF TECH WRIGHT-PATTERSON AFB OH
J R ROGACKI 1983 AFIT/CI/NR-83-34T

UNCLASSIFIED F/G 11/6 NL

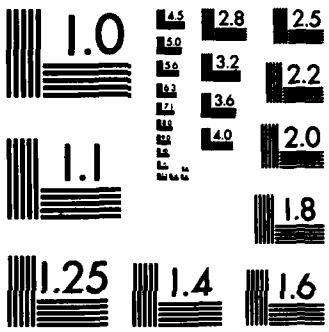

MICROCOPY RESOLUTION TEST CHART
NATIONAL BUREAU OF STANDARDS-1963-A

be seen that Ps can be approximated by an equation of the form:

$$Ps = C3\ f^{C4} \qquad \text{(Eqn. 5.3)}$$

where, in this case, C3 = 0.98 and C4 = -0.53, f is given in meters per pass, and Ps has the units Nm/g.

Three points deviate from the line in Fig. 5.17. Points labeled "a" and "b" represent results from tests #21 and 23 which used square ended blades at large feeds. In these tests the seal material was cut away, and little densification took place. Point "c" is from test #11, which had an extremely low coefficient of friction (0.21). It is suspected that the seal specimen was lubricated by some unknown contaminant prior to or during the test, thus reducing the tangential force.

Three important facts can be learned from Fig. 5.17:

1. Fig. 5.17 clearly shows that Ps decreases substantially as feed is increased.
2. Ps is considerably lower when the seal material is cut rather than worn away.
3. Ps is slightly higher for square ended blades than for slanted blades.

Consideration of Wear Mechanisms

Eight wear mechanisms were discussed in Chapter IV, and three of these were said to apply directly to the rub

interaction between turbine blades and seals: abrasion, adhesion, and fatigue.

During the low speed tests, when the blade tip leading edge radius was small compared to the feed (see "Effects of Blade Tip Radius"), the seal material was cut away with little densification. As the feed was decreased, or the leading edge radius increased, abrasion of the seal material became almost negligible.

It is hypothesized that the primary mechanism of seal material removal, in those cases when cutting did not occur, was fatigue. Several factors point toward this conclusion. First, because the seal material is made from a sintered powder, the voids and junctions provide excellent locations for the initiation of fatigue cracks. Second, as the blade passes over a particular area of the seal, the particles in that area are subjected to cyclical loading - compression followed by tension - as described in Chapter IV. Third, those seal specimens in tests which had low feeds (e.g. #26 - 28) exhibited less densification (and more wear) than those from high feed tests (e.g. #21 - 23). This shows that wear was related to the number of passes, or loading cycles. Finally, a fatigue phenomenon was repeatedly observed during the rub tests. The surface of the seal material would initially densify in discrete patches; then, as rubbing continued, these patches were removed and new ones formed. Since this phenomenon occured

at both high and low forces, the cyclical nature of fatigue wear is again suggested.

Movies of Rub Interaction

The 16mm movies taken during rub testing proved ineffective in studying the blade/seal rub interaction. A more sophisticated camera, capable of higher magnification and greater depth of field, is needed to produce useable pictures.

CHAPTER VI

CONCLUSIONS

The following conclusions may be drawn as a result of the work done during this study.

1. The modulus of elasticity (E) of the seal material varies with strain. As the material is compressed, E increases, and as the material is stretched, E decreases. E can be estimated for a given amount of strain (e) by the equation:

$$E = E_o \times 10^{C2\ e}$$

where $E_o = 2.95 \times 10^{3} MN/m^2$ (i.e. E at zero densification), and C 2 = -1.96.

2. The normal force, Fn, between the blade and seal varies with the amount of smearing at the rub interface. Smeared areas result in higher forces than unsmeared areas.

3. Forces do not vary significantly with rub velocity within the range of velocities tested during this work. Furthermore, forces recorded during low speed rub testing were of the same order of magnitude as those recorded by researchers during high speed (100 m/s) rub testing.

4. In general, increasing feed resulted in greater forces, with two exceptions. First, when rubbed by square-ended blades at feeds which were large compared to the blade tip leading edge radius, the seal material was cut away with little densification, and the forces remained approximately constant. Second, at extremely low feeds (0.63×10^{-6} m/pass or less), the seal material was worn away at approximately the same rate as it was densified, so forces again remained constant.

5. Blades having a blade tip lay perpendicular to rubbing produced higher tangential forces, a higher coefficient of friction, and less densification than blades whose lay was parallel to rubbing.

6. The seal material is history dependent. Forces encountered during a particular rub are affected by the amount of densification (or smearing) caused by previous rubs.

7. When feed is stopped but rubbing is permitted to continue, the elastic forces in the system decay exponentially, according to the equation:

$$Fn = Fn_o^{(10^{(-DN)})}$$

where N is the number of passes since the incursion was

stopped, Fn is the normal force when the incursion was stopped, and D is a constant.

8. The specific energy of material displacement, Ps, varies with feed, f, according to the equation:

$$Ps = C3\ f^{-C4}$$

where C3 and C4 are constants.

9. The primary mechanism of seal material wear (in the absence of cutting) is fatigue.

10. Fn varies with blade tip area.

11. Further work should be done, however, in studying the effects of blade tip area on forces, seal material densification, and specific energy of seal material displacement.

REFERENCES

1. N.L.Mochel, "Wear in Steam Engines", Mechanical Wear, American Society for Metals, 1950.

2. L.P.Ludwig, R.C.Bill, "Gas Path Sealing in Turbine Engines", NASA Technical Memorandum 73890 (Revised), 1978.

3. R.C.Bill, L.P.Ludwig, "Wear of Seal Materials Used in Aircraft Propulsion Systems", Paper Presented at the Workshop on Thermal Deformation, Annapolis, Md., 1979.

4. J.L.Jefferson, R.C.Turner, "Some Shrouding and Tip Clearance Effects in Axial Flow Compressors", International Shipbuilding Progress, Vol. 5, No. 42, Feb 1958.

5. D.P.Fleming, "Rotor Bearing Dynamics of Modern Turbomachinery", Tribology International, 1980.

6. R.C.Bill, L.T.Shiembob,"Friction and Wear of Sintered Fibermetal Abradable Seal Materials", NASA TMX-73659, 1977.

7. J.G.Ferguson, "Use of Coatings in Turbomachinery Gas Path Seals", AGARD Conference Proceedings No. 237: Seal Technology in Gas Turbine Engines, 1978.

8. J.W.Vogan, N.C.Solomon, A.R.Stetson, "Advanced Ceramic Materials for High Temperature Turbine Tip Seals", NASA CR-159774, 1980.

9. J.Wolak, A.F.Emery, S.Etemad, S.R.Choi, "Preliminary Results on the Abradability of Porous, Sintered, Seal Material", ASME/ASLE Joint Lubrication Conference, Washington D.C., Oct. 5-7, 1982, Paper 82-Lub-7.

10. R.C.Bill, D.W.Wisander, "Friction and Wear of Several Compressor Gas-Path Seal Materials", NASA TP-1128, 1978.

11. W.F.Laverty, "Compressor Seal Rub Energetics Study Final Report", NASA CR-159424, 1978.

12. S.R.Choi, "High Intensity Rubbing Process of a Porous Body As a Function of the Geometry of the Contacting Surface", Master of Science Thesis, University of Washington, Seattle, 1983.

13. 1982 Annual Book of ASTM Standards, Part 10, ASTM, Philadelphia, 1982.

14. P.Albrecht,"New Developments in the Theory of the Metal Cutting Process: The Ploughing Process in Metal Cutting", Trans ASME, 59-A-243, 1959.

15. D.H.Buckley, Surface Effects in Adhesion, Friction, Wear, and Lubrication, Elsevier Scientific Publishing Co., New York, 1981.

16. M.M.Saverin, in Friction and Wear Calculation Methods, Pergamon Press, Elmsford, N.Y., 1982, p 257.

17. A.D.Sarkar, Friction and Wear, Academic Press, New York, 1980.

18. Tribology Handbook, M.J.Neall Ed., Butterworths, London, 1973.

19. R.T.Spurr, "The Abrasive Wear of Metals", Wear (65), Lausanne, Netherlands, 1981.

20. D.F.Moore, Principles and Applications of Tribology, Pergamon Press, New York, 1975.

21. L.H.Van Vlack, Elements of Materials Science, Addison-Wesley Publishing Co., Inc., Reading, Mass., 1959.

22. J.Wolak,A.F.Emery,S.Etemad,S.R. Choi, "Blade Tip Geometry - A Factor in Abrading Sintered Seal Material", paper submitted for review by ASME, 1983.

APPENDIX A

EQUIPMENT CALIBRATION

Force Measuring Equipment

The force measuring equipment (dynamometers, amplifiers and chart recorder) was calibrated prior to the start of rub testing and rechecked after the testing was completed. The equipment was calibrated for normal and tangential forces at several different chart recorder sensitivity settings. Amplifier gain settings were set to the values used during the tests: strain gage dynamometer amplifier gain was set to 2500X for both Ft and Fn; Kistler charge amplifier setting was .5mV/pc for Ft; and Kistler charge amplifier setting was 5N/div for Fn.

Both dynamometers were calibrated for tangential forces by using a Chatillon force gage (Model DPPH 250). Ft was simulated by applying a force against one arm of the force gage by turning a screw which passed through a fixture secured to the planer table. The force was measured by the force gage and transmitted to either a blade mounted in the strain gage dynamometer or a plate bolted to the top of the Kistler dynamometer, depending on which dynamometer was being calibrated. (See Fig A.1.) Ft was applied in increments of 10 to 25 lbs and recorded by the chart recorder.

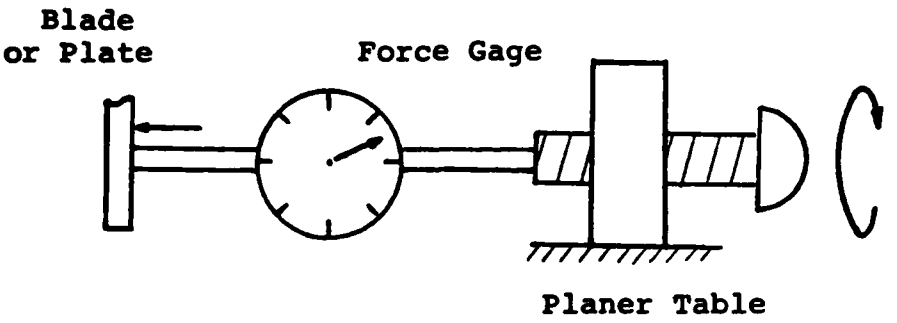

Fig. A.1 - Calibration of dynamometers using screw and force gage.

The Kistler dynamometer was calibrated for normal force by applying weights directly to a plate mounted to the dynamometer surface. The strain gage dynamometer was calibrated for Fn through a lever and fulcrum. The fulcrum was positioned on the planer table top and one end of the lever arm placed under a blade mounted in the dynamometer. Weights were then added to a bracket positioned on the other end of the lever arm, resulting in an upward normal force against the blade.

Results of the calibration are shown in Figs. A.2 through A.5.

Calibration of Instron Testing Instrument

After an initial warm-up of at least one hour, the Instron testing instrument was calibrated according to the

manufacturer's operating instructions, as found in Instron Manual 10-29-1 (A). The instrument was first zeroed and then balanced as prescribed. Next, the upper grip was removed from the load cell, and the calibration hanger was installed. Calibrating weights of 5 Kg each were added to the hanger to a total of 25 Kg. As each weight was added, the calibrating control knob was rotated as necessary to position the pen at the desired division on the chart. With the Load Selector Switch in the "1" position, the load cell provided full scale deflection at 50 Kg force. See Instron Manual 10-29-1 (A) for more detailed instructions and photographs.

Calibration of Extensometer

Upon completion of the calibration of the Instron testing instrument, the strain gage extensometer was calibrated according to the instructions found in Instron Manual 10-69-1 (A). The extensometer was mounted onto a micrometer as prescribed, with the extensometer cable connected to the strain gage preamplifier on the X-Y Chart Drive System. The extensometer was then balanced using balance controls on the strain gage preamplifier. Next, the extensometer was extended to 0.5mm in 0.1mm increments by adjusting the micrometer, and the 0.1mm increments were marked on the chart used subsequently in the tensile test. 0.1mm extension on the extensometer corresponded to a

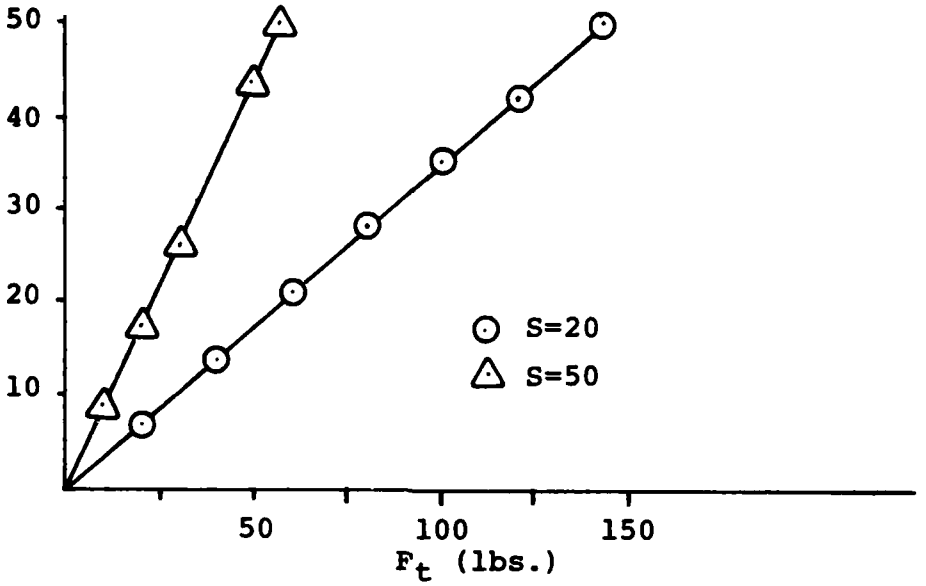

Fig. A.2 - Calibration of Kistler dynamometer in F_t direction. S is the sensitivity setting on the chart recorder.

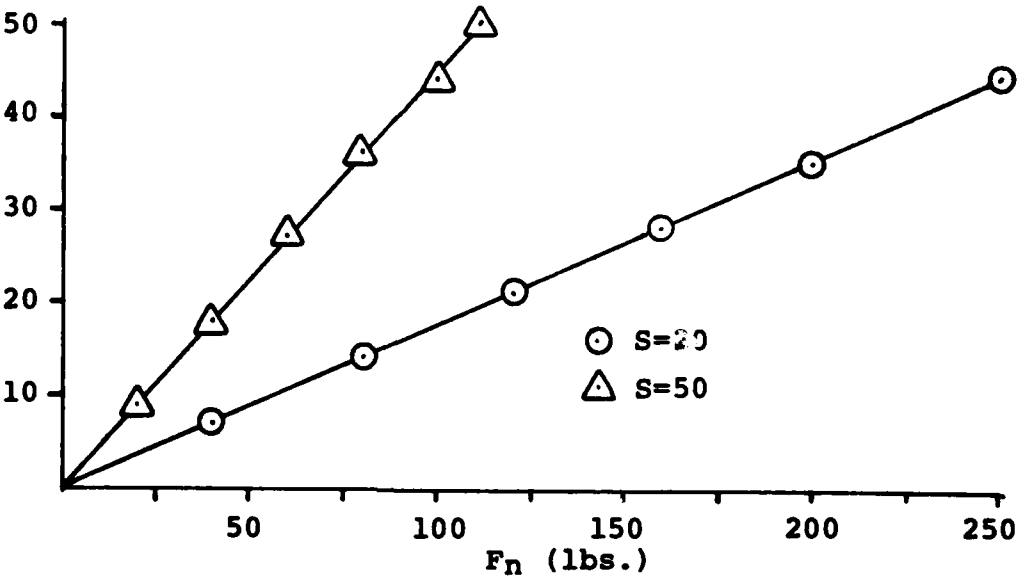

Fig. A.3 - Calibration of Kistler dynamometer in F_n direction.

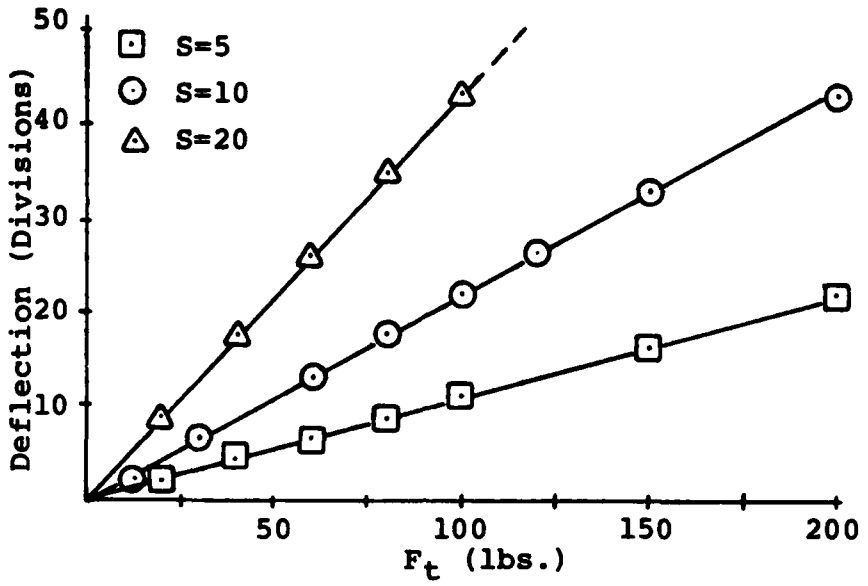

Fig. A.4 - Calibration of strain gage dynamometer in F_t direction. S is the sensitivity setting on the chart recorder.

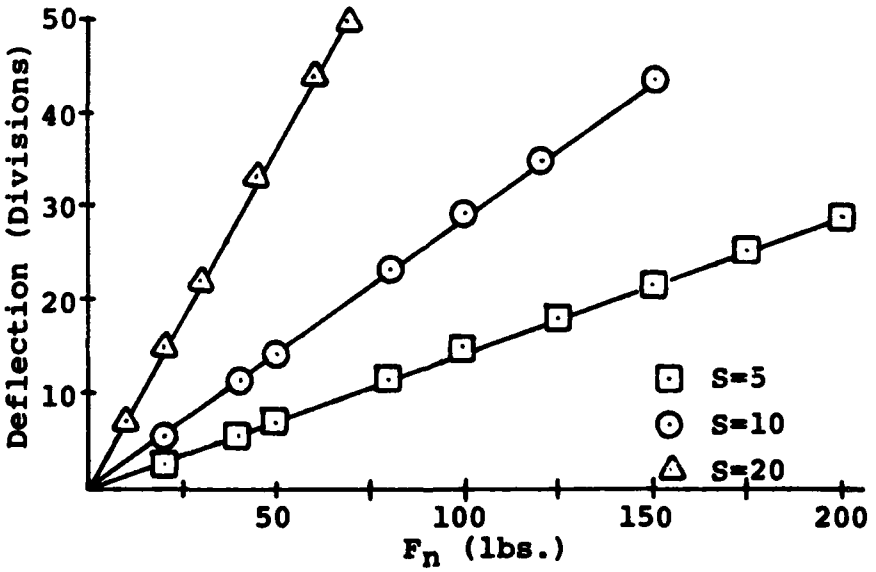

Fig. A.5 - Calibration of strain gage dynamometer in F_n direction.

chart deflection of approximately 25.3 divisions. Since the gage length was 1 inch, each division represented a strain of 0.156%. See Instron Manual 10-69-1 (A) for additional details and photographs.

APPENDIX B

Calculation of Seal Densification Factor

The seal densification factor, Sd, as defined by Wolak et al (9) is as follows:

$$Sd = \frac{Wg - Ws}{Wg}$$

where Ws is the weight loss of seal material through rubbing to generate the groove. Ws was found by comparing the weight of the seal before and after the rub test. Wg is the weight of undisturbed material equal in volume to the volume of the groove made in the seal during rubbing. Wg was found by calculating the volume of the groove and multiplying that volume by the average density of the seal material.

The volume of the rub groove, Vg, can be expressed by:

$$Vg = w\,(dL\ I + I^2\ (1\ /\ \tan B\ ))$$

where w is the width of the groove (normally 1.27cm), I is the total incursion during the rub test, L is the length of the top surface of the seal before rubbing, and B is the chamfer angle of the seal specimen (either 15 or 20 degrees, depending on the particular specimen). These dimensions are shown in Fig B.1.

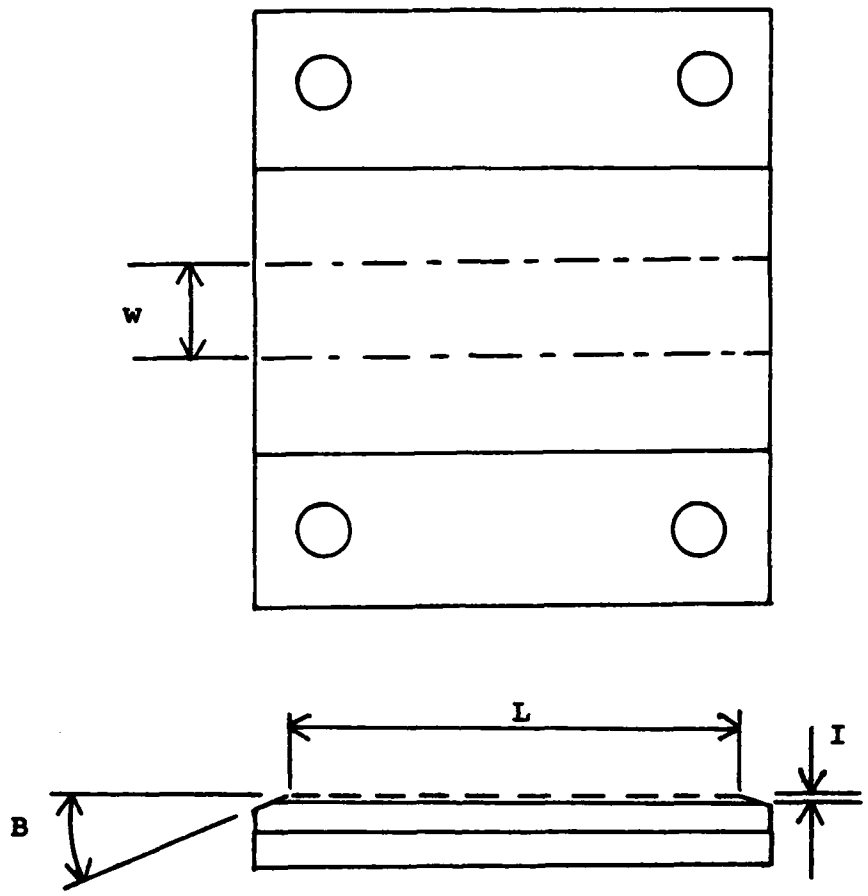

Fig. B.1 -Dimensions of seal specimen used in calculating the seal densification factor, S_d.

APPENDIX C

DERIVATION OF EQUATIONS

Modulus of Elasticity/Strain (Eqn 5.1)

The curve in Fig. 5.2 is of the form:

$$y = 10^{C2x}$$

or: $$(C1)\ E = 10^{C2e}$$

At e = 0, (C1) E = 1, so:

$$C1 = 1/E_o$$

where E_o = 2.95 MN/m^2 (the value of E at e = 0). Solving for C2,

$$C2 = -1.96$$

therefore $$E = 2.95 \times 10^{-1.96e}$$

Decay of Fn at Zero Feed (Eqn 5.2)

The curve in Fig.5.14 is of the form:

$$y = mx + b$$

or: $$\log(\log(Fn)) = (m)\ N + \log(\log(Fn_o)).$$

Solving graphically, m = -0.0027 .

Therefore, $$\log(Fn) = \log Fn_o\, 10^{(-0.0027N)}$$

or $$Fn = Fn_o^{(10^{(-0.0027N)})}.$$

Specific Energy of Material Displacement (Eqn 5.3)

The specific energy of material displacement (Ps) is defined as the energy (El) required to displace a given weight of seal material (W):

$$Ps = El/W$$

where W = volume X density

and El = Ft X rub length.

The curve in Fig. 5.17 is of the form:

$$y = (m)x + b$$

or $$\ln(f) = C3 \ln(Ps) + C4.$$

Solving for C3 and C4 graphically and substituting,

$$Ps = 0.98\ f^{-0.53}\ .$$

END

FILMED

10-83

DTIC